Doctoral Thesis

CONSTRUCTION OF ISOTROPIC CELLULAR AUTOMATON AND ITS APPLICATION

(等方セルオートマトンの構成とその応用)

AKINOBU NISHIYAMA
Graduate School of Mathematical Sciences, The University of Tokyo

January 2010

Contents

1 Introduction

Reaction-diffusion equations are used extensively for modelling pattern formation observed in natural and social phenomena. The equations are deduced from the simple idea that concentration changes of a material in a system are caused by reactions between the materials contained in the system and by diffusion of each material. Numerical solutions of the equations show a variety of patterns, and they are used widely in various fields such as chemistry, biology, medical science etc. [1].

An alternative approach to modelling pattern formation is to use a cellular automaton (CA) [2, 3]. CAs are mathematical models with discrete time, space and state variables, and are defined by simple time evolution rules. They are able to reproduce complex patterns, and therefore have a lot of applications. For example, the lattice gas CAs represent very well the various features of fluid dynamics and reaction-diffusion phenomena [4]. In general, CAs have the advantage of being able to simulate phenomena at lower computational cost than when using partial differential equations.

A lot of models for cooperative phenomena of excitable media, derived by using partial differential equations or cellular automata have been proposed. The so-called "oregonator" model [6, 7, 8] expressed in terms of differential equations can explain the Belousov-Zhabotinsky(BZ) reaction [5] known as a typical example of a reaction-diffusion system. On the other hand, some approaches by means of cellular automata for excitable media have been proposed in [9, 10, 11]. However, these early CA models featured update rules based on nearest neighbour connections, and hence, faced several serious shortcomings [12]. The most serious of these is the lack of curvature and dispersion effects and unwanted anisotropy of the front motion [13, 14]. To overcome these problems, several automata models have been proposed [13, 15, 16, 14, 18, 19]. Gerhardt, Shuster and Tyson introduced bigger neighbourhoods to model the curvature effects and make the threshold a linear function to take dispersion into account [13, 15, 16]. Weimar, Tyson and Watson improved the models by introducing a mask, i.e. a weighted summation of automaton values over large neighbourhoods [18, 19], and Henze and Tyson extended it to three spatial dimensions [20]. These models recover curvature and dispersion effects well, but the anisotropy of wave propagation is not completely eliminated.

In cellular automata, to recover the isotropy of the time-evolution patterns is in fact a difficult problem. If the adopted lattice used in the modelling has periodicity,

such as a square lattice or a hexagonal lattice, then, due to this periodicity the time-evolution patterns obtained from the model become anisotropic. In [17] Markus and Hess have proposed an isotropic model for excitable media. In their model, they use a square lattice, but instead of placing each grid point at the center of a unit cell, they assign each grid point to a random location within its unit cell. The isotropy is recovered by taking a large number of neighbouring cells within a circular area with radius R. As other CA models for excitable media which seem to recover anisotropy to some extent, one can cite the "Moving Average CA" method by Weimar [22], the lattice gas method CAs by Raymond et al. [23] or Chen [24] et al., the isotropic CA model for the growth process of a bacterial colony by using a Voronoi lattice [25] proposed in [26].

However, the work that addressed the anisotropy of cellular automata are hardly known. We focus on the isotropy of the model and want to address this problem. In the present thesis, we discuss the isotropy of model, and propose some isotropic cellular automata.

In chapter 2, we propose a cellular automaton model, which reproduces isotropic time-evolution patterns observed in the Belousov-Zhabotinsky reaction. Although several CA models have been proposed exhibiting isotropic patterns of the reaction, most of them need complicated rules and a large number of neighbouring cells. Our model can produce isotropic patterns from a simple probabilistic rule among a few (4 or 8) neighbouring cells.

In chapter 3, we propose a new method to construct an isotropic cellular automaton corresponding to a reaction-diffusion equation. The method consists of replacing the diffusion term and the reaction term of the reaction-diffusion equation with a random walk of microscopic particles and a discrete vector field which defines the time evolution of the particles. The cellular automaton thus obtained can retain isotropy and therefore reproduces the patterns found in the numerical solutions of the reaction-diffusion equation. As a specific example, we apply the method to the Belousov-Zhabotinsky reaction in excitable media.

In chapter 4, we present a model which aims at describing the morphology of colonies of *Proteus mirabilis* and *Bacillus subtilis*. Our model is based on the isotropic cellular automaton introduced in chapter 3. The cellular automaton which is obtained by the adequate discretisation of a diffusion-like equation, describing the migration of the bacteria, to which we have added rules simulating the consolidation process. Our basic assumption, following the findings of the group of Chuo

University, is that the migration and consolidation processes are controlled by the local density of the bacteria. We show that it is possible, within our model to reproduce the morphological diagrams of both bacteria species. Moreover we model some detailed experiments of the precited group, obtaining a fine agreement.

2 An isotropic cellular automaton model for excitable media

In this chapter, we propose an isotropic cellular automaton for excitable media. Firstly, we explain two approaches modelling excitable media.

2.1 Modelling of excitable media

The Belousov-Zhabotinsky (BZ) reaction observed in excited media is a typical example of oscillatory phenomena in reaction-diffusion systems. It exhibits interesting behaviour such as target patterns and spiral patterns under certain conditions [5]. Figures 1 (a) and 1 (b) show the target pattern and the spiral pattern in the Belousov-Zhabotinsky reaction respectively [27]. Excitable media are often modeled by so-called reaction-diffusion equations, described as simultaneous differential equations,

$$\begin{aligned} u_t &= f(u,v) + D_u \Delta u \\ v_t &= g(u,v) + D_v \Delta v, \end{aligned} \tag{1}$$

where $u(x,y,t)$, $v(x,y,t)$ are state variables corresponding to the concentrations of two kinds of medium. D_u and D_v are diffusion coefficients. The functions $f(u,v)$ and $g(u,v)$ are reaction terms which describe the interaction between u and v [28]. Figure 2 shows a typical phase diagram for the BZ reaction. The phase diagram has an equilibrium point at the intersection of two nullclines $f(u,v) = 0$ and $g(u,v) = 0$. Although the state at the equilibrium point is stable under weak perturbation, if the strength of the perturbation due mainly to the diffusion effects exceeds a certain threshold, it becomes unstable and changes along the line shown in the phase diagram until it returns to the equilibrium point again. Hence, the state variables determined by the above reaction-diffusion equations reproduce the specific patterns of excitable media quite well.

An alternative approach to model excitable media is by means of a cellular automaton (CA) [2]. CAs are mathematical models with discrete time, space and state variables, and are defined by simple evolution rules. Accordingly, CAs have the benefit of being able to reproduce complex patterns at low computational cost.

An isotropic model for excitable media was proposed by Markus and Hess[14]. In their model, they use a rectangular lattice, but instead of placing each grid point at

the center of a unit cell, they assign each grid point to a random location within its unit cell. The isotropy is recovered by taking a large number of neighbouring cells within a circular area with a radius R (Figure 3). This CA succeeded in describing the isotropic nature of the observed phenomena (Figure 4). However, the practical calculation of the model requires large computational resources, because it needs lookups of the random points and additions of state variables over wide-ranging neighbouring cells.

The purpose of the present chapter is to propose an isotropic CA model with only a few (4 or 8) neighbouring cells. We shall show that it reproduces the behaviour of excitable media with less computational time than the model by Markus and Hess.

2.2 The CA model

In this section, we describe a CA rule which reproduces isotropic patterns for excitable media. Our isotropic model is constructed in two steps. Firstly, an anisotropic square lattice model is shown in section 2.2.1. It is an improvement for a model which was proposed in [29]. We discuss the nature of the patterns and obtain some important results regarding the construction of an isotropic pattern. Secondly, the method to recover isotropy is proposed in section 2.2.2. on the basis of the results presented in section 2.2.1.

2.2.1 Simple square lattice model

Firstly, we introduce a simple square lattice model which gives some anisotropic patterns. It models the dynamics of reaction-diffusion equation already introduced in section 2.1. The model is defined on a 2-dimensional square lattice. Each cell has two state variables u^t_{mn} and v^t_{mn}, where m, n, and t denotes the column number, row number, and the time step, respectively. Each of the state variables takes a value from 0 to $N-1$. The time-evolution rule is defined by the sum of values of the states u^t_{mn} at the time t over the Moore neighbouring cells;

$$\begin{aligned} S^t_{mn} &:= u^t_{m-1,n-1} + u^t_{m,n-1} + u^t_{m+1,n-1} + u^t_{m-1,n} \\ &+ u^t_{m+1,n} + u^t_{m-1,n+1} + u^t_{m,n+1} + u^t_{m+1,n+1}. \end{aligned}$$

Figure 5 explains the time-evolution rule for each cell. The state of each cell at time $t+1$ is determined by the following rules. (1) If $u^t_{mn} = v^t_{mn} = 0$ and $S^t_{mn} \geq \Delta$,

then u^t_{mn} is excited to $u^t_{mn} = 1$, while v^t_{mn} stays $v^t_{mn} = 0$. Else, if $u^t_{mn} = v^t_{mn} = 0$ and $S^t_{mn} < \Delta$ each state stays $u^t_{mn} = v^t_{mn} = 0$. (2) If $u^t_{mn} + v^t_{mn} \neq 0$ then the values at the cell automatically transit to the next point along the line indicated by the arrow in the diagram (Fig.5) (and finally return to $u^t_{mn} = v^t_{mn} = 0$). The Δ is a threshold for the excitation, and is a positive constant ($\Delta > 0$). This rule can be interpreted as saying that if there is a flow larger than a threshold into a cell, then the cell oscillates only once. It is a simple emulation of the dynamics described by the phase diagram in Fig.2. The model described above gives a variety of patterns, such as ring patterns, target patterns and spiral patterns, for appropriate initial conditions. Figure 6 shows an example of target patterns obtained from the above rule. These two patterns are computed using different thresholds, (a) $\Delta = 3$ and (b) $\Delta = 6$. At this stage, these patterns are not isotropic yet. However, there are some remarkable relationships between the threshold Δ and the obtained pattern, that are important for constructing isotropic patterns in the next section.

(i) The symmetry (and therefore the anisotropy) of the obtained pattern only depends on the value of the threshold Δ, not on the number of states N. For example, an octagonal pattern is obtained for $\Delta = 3$, and a dodecagonal pattern for $\Delta = 6$ as shown in Fig.6. Table 1 shows the threshold dependency of the shape of the pattern.

(ii) The propagation speed of the wave front for the obtained patterns is determined by the value of the threshold Δ but not by N. The patterns in Fig.6 (a) and (b) were obtained after the same number of time steps, with $\Delta = 3$ and $\Delta = 6$, respectively. This indicates that the lower threshold triggered a faster excitation. Figure 7 shows the propagation speed of the wave front plotted as a function of the threshold Δ. It is inversely proportional to the threshold Δ, and can be approximated by the equation $v = 1/(0.59577 + 0.32493\ \Delta)$. Note that as the propagation speed in fact depends on the direction, we defined an average propagation speed by averaging the measurements over the angle.

(iii) There are two control parameters Δ and N in this model. To generate a pattern, it is necessary to choose a threshold in the range $0 < \Delta < 2N$, otherwise the excitation does not take place over the whole range of cells. Thus the number of state values N is relevant only when deciding the range of the thresholds Δ, and it does not have a dominant influence on the system. We can control the shape and propagation speed of the generated patterns by choosing an appropriate value of the threshold.

2.2.2 Isotropic square lattice model

In this section, we introduce a CA model that generates an isotropic pattern using the features discussed in section 2.2.1. This is accomplished by introducing a randomness into the model. We prepare two different thresholds Δ_1 and Δ_2 ($\Delta_1 > \Delta_2 \neq 0$). These are distributed randomly over the cells at the beginning of the simulation and are kept constant during the simulation (Fig.8(a)). The procedure is summarized as follows,

$$\Delta_{mn} := \begin{cases} \Delta_1 & p \\ \Delta_2 & q \equiv 1 - p \end{cases} \tag{2}$$

where p is the probability that Δ_1 is assigned to a cell. The time-evolution rule is the same as that for the model described in section 2.2.1, except for replacing the threshold Δ with Δ_{mn}. Namely, the excitation condition is replaced by $S^t_{mn} \geq \Delta_{mn}$ (Fig.8(b)). This results in each cell possessing one of two different transition speeds, according to the threshold randomly assigned to the cell. It is expected that this difference breaks the anisotropy resulting from the periodicity of the original lattice.

2.3 Numerical results

In this section, we show some numerical results obtained from our isotropic model and discuss them.

First we compare the computational time required for updating a cell of our model and that of the model by Markus and Hess. Let T_i, T_m, T_p and T_s be computational times for a step of conditional bifurcation, multiplication, addition and substitution respectively. Then our model requires about

$$\sim 5T_i + 2T_s + 8T_p$$

for updating one cell. On the other hand, their model requires

$$\sim (T_i + T_s + T_p)\pi R^2 + 2T_i + T_s + T_m$$

where R is the radius of the circular region of neighbouring cells. In general, we can assume $T_i \gg T_m, T_p, T_s$, the ratio of computational time is approximately $5 : \pi R^2$. Since the radius R is typically taken from 6 to 10, our model is more than 20 times faster than their model.

Figures 9 $\sim$ 14 show some typical examples of patterns obtained by numerical computation. They are plotted in grey scale according to the value of u^t_{mn} from 0 (black) to $N-1$ (white).

The first example is a single ring pattern (Fig.9(a)). It is produced by the initial condition $u^0_{mn} = 1$ and $v^0_{mn} = 0$ on 3×3 cells at the center and $u^0_{mn} = v^0_{mn} = 0$ on the other cells. From the central 3×3 cells, a ring-shaped wave spreads outward. We evaluated the anisotropy of the pattern by measuring the residual error when compared to the average radius of the ring, and plotted it as a function of the propagation direction in Fig.9(b). We can see that the wave fronts of the ring pattern propagate uniformly in each direction. In Fig.10 we plotted the variation from the circle as a function of the radius of the ring pattern. It shows that the ring pattern indeed grows closer to a complete circle as the radius (and therefore the time step) increases.

The next example is a target pattern (Fig.11). The initial condition is $u^0_{mn} = 1$ and $v^0_{mn} = 0$ on the central cell and $u^0_{mn} = v^0_{mn} = 0$ on the other cells. From the central cell, ring-shaped waves are produced that spread repeatedly with a spatial period of $4(N-1)$, and a target pattern is formed. In order to generate a spiral pattern, appropriate initial conditions are needed. Firstly, we generate a single ring pattern like the one in Fig.9(a). Then we cut off one part of the ring pattern as shown in Fig.12(a) and use the remainder as the initial state. In fact, spiral patterns are also observed cutting a part of ring patterns in experiments on the Belousov-Zhabotinsky reaction [6]. The spiral pattern obtained from our model is shown in Fig.12(b). The isotropic feature of the pattern is apparent.

When we take random initial conditions, in general many target patterns appear. An example is shown in Fig.13. Figure 14 shows an example of a target pattern for a large value of N ($N = 200$), with $\Delta_1 = 10$, $\Delta_2 = 400$. The boundaries of the pattern exhibit complicated shapes like the DLA cluster [31].

2.4 Summary

In this chapter, we proposed a simple CA model for excitable media which can generate isotropic patterns though it is defined on the square lattice and its time-evolution rule depends only on the Moore neighbourhood. The key to isotropy is to introduce spatial randomness of the excitation threshold in the model. As the propagation speed and direction of the patterns are strongly affected by changes in the values of

the thresholds, the randomness of the threshold at each cell causes fluctuations in the pattern formation, which seem to make the pattern isotropic. Using this model, we have successfully reproduced isotropic patterns observed in excitable media such as target patterns and spiral patterns. Application to higher dimensional CA models and application to inverse ultradiscretization [32] are important problems we wish to address in future.

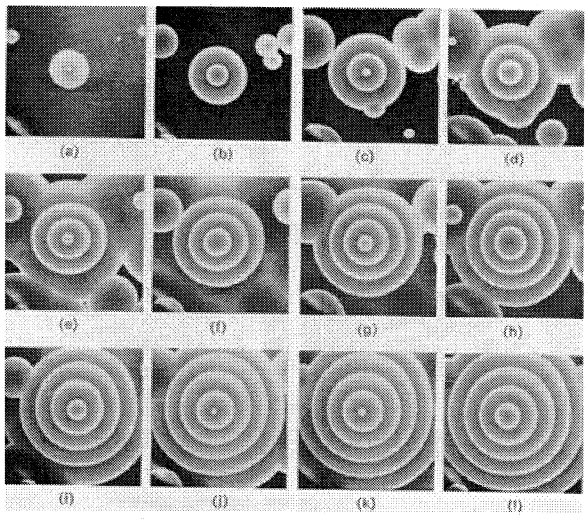

(a)

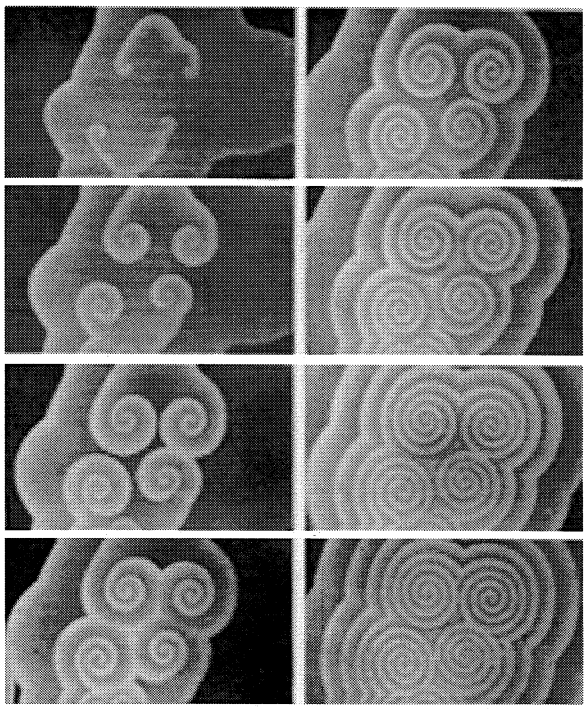

(b)

Figure 1: The patterns observed in the Belousov-Zhabotinsky reaction [27]. (a) Target pattern. (b) Spiral pattern.

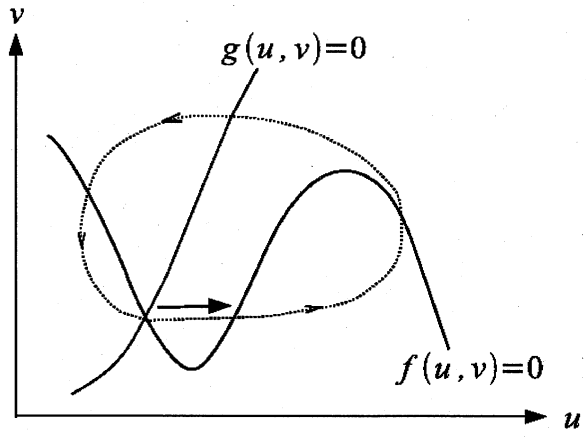

Figure 2: Typical phase diagram for the BZ reaction.

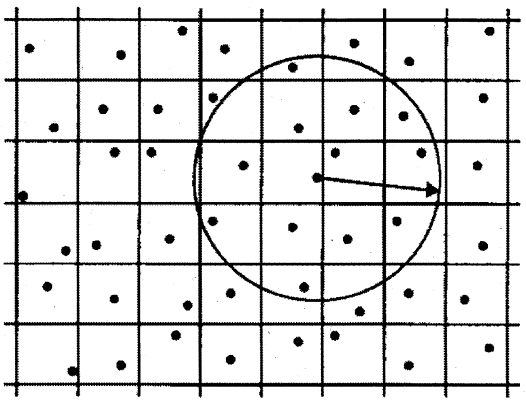

Figure 3: Geometry of Markus's cellular automaton[30]. The plane is divided into square cells and one point is placed randomly in each cell. The circular neighbourhood of a cell is defined by all cells whose point is within a circle centered at that point.

Figure 4: The spiral waves obtained from Markus's cellular automaton (128 $\times$ 128 cells) [30].

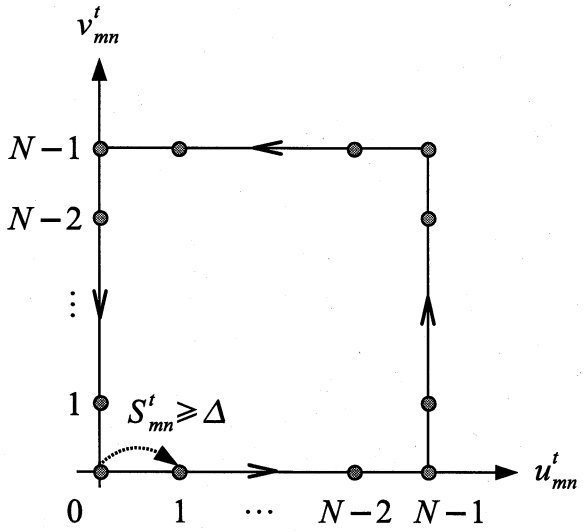

Figure 5: Phase diagram which gives the time-evolution rule for u^t_{mn} and v^t_{mn}. This diagram is simply an imitation of the phase diagram of Fig.2.

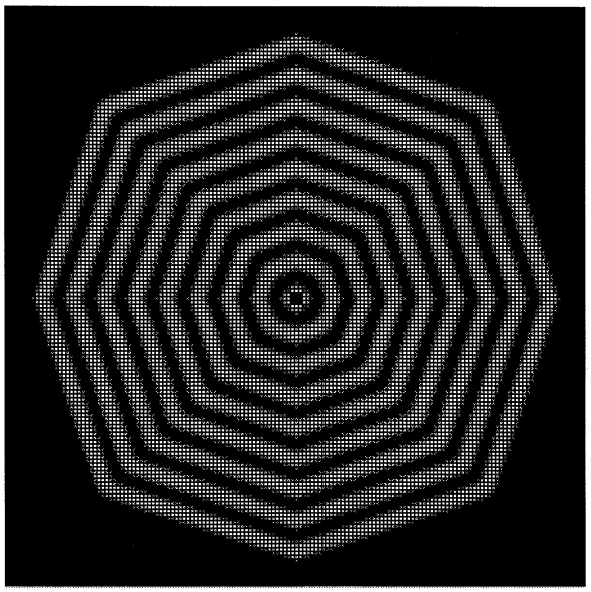

(a)

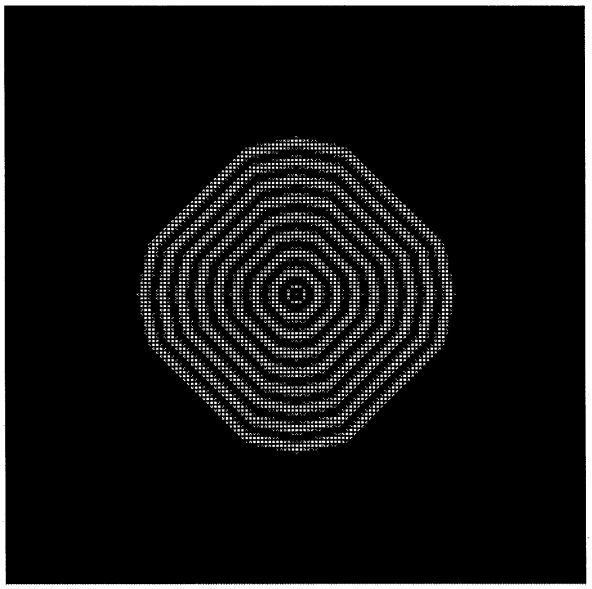

(b)

Figure 6: Anisotropic target patterns obtained from the simple square lattice model. (a) 150×150 cells, $t = 100$, $N = 4$, $\Delta = 3$. (b) 150×150 cells, $t = 100$, $N = 4$, $\Delta = 6$.

Table 1: Threshold Δ dependency on the symmetry of the obtained patterns.

Threshold Δ	The symmetry of the pattern
1	quadrilateral
2	quadrilateral
3	octagon
4	octagon
5	octagon
6	dodecagon
7	octagon
8	octagon
9	hexadecagon
10	dodecagon
11	octagon
12	hexadecagon
$\vdots$	$\vdots$

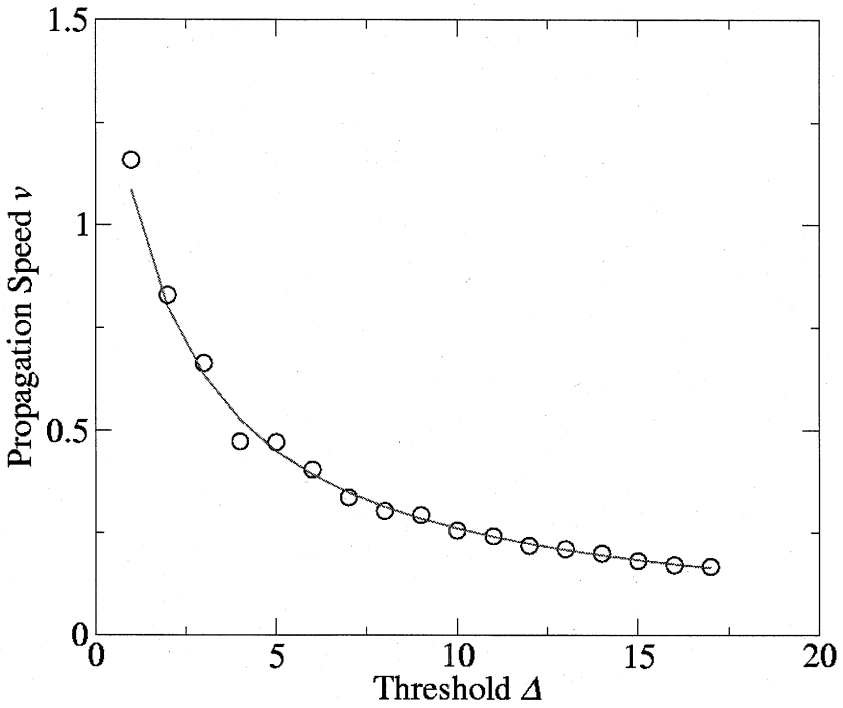

Figure 7: The average propagation speed v of the patterns as a function of the threshold Δ. It can be approximated by $v = 1/(0.59577 + 0.32493\ \Delta)$.

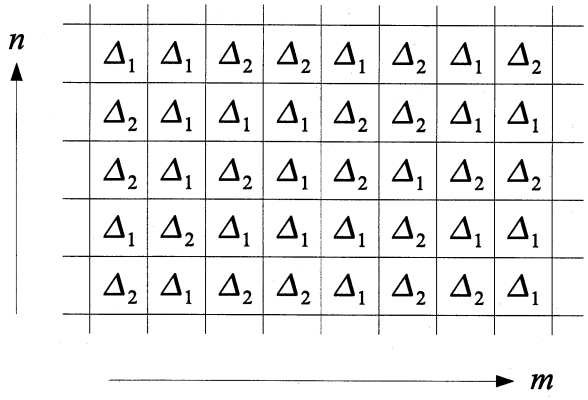

(a)

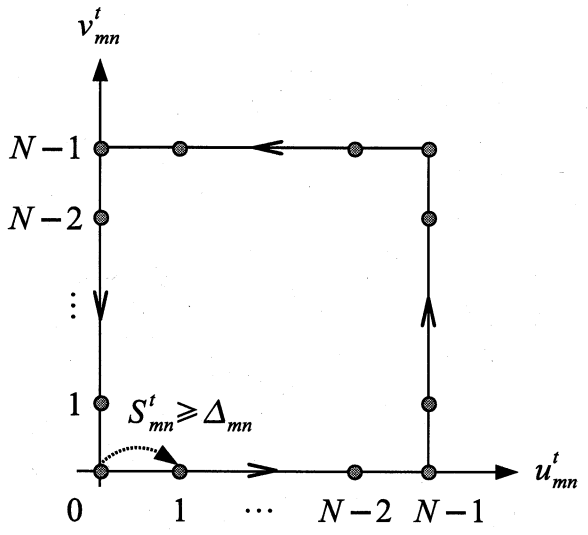

(b)

Figure 8: (a) Example of an arrangement of thresholds Δ_{mn}. The thresholds Δ_1 or Δ_2 are distributed randomly over the lattice. (b) The time-evolution rules almost the same as for the model in section 2.2.1: The excitation condition is however replaced by $S^t_{mn} \geq \Delta_{mn}$.

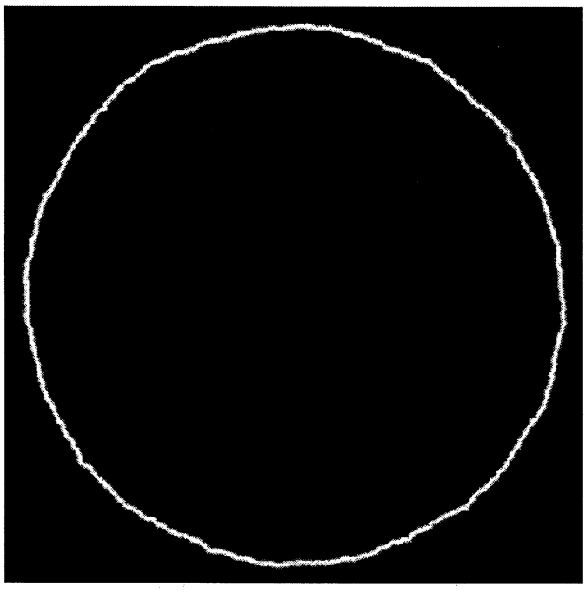

(a)

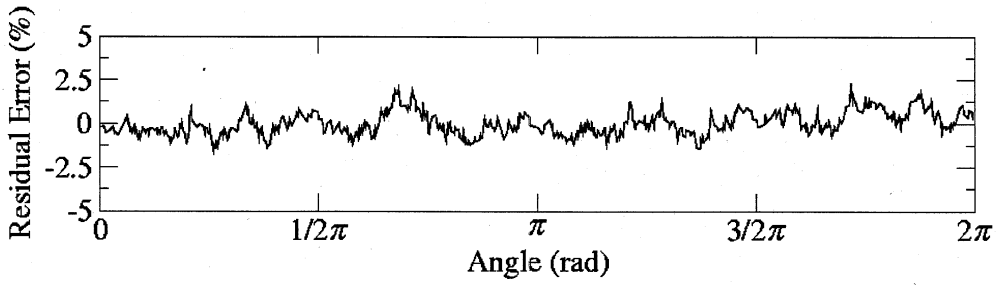

(b)

Figure 9: (a) Single ring pattern for 500×500 cells, $t = 450$, $N = 5$, $\Delta_1 = 3$, $\Delta_2 = 7$, $p = 1/2$. (b) Plot of the anisotropy of the model, measured as the residual error of the ring pattern in (a).

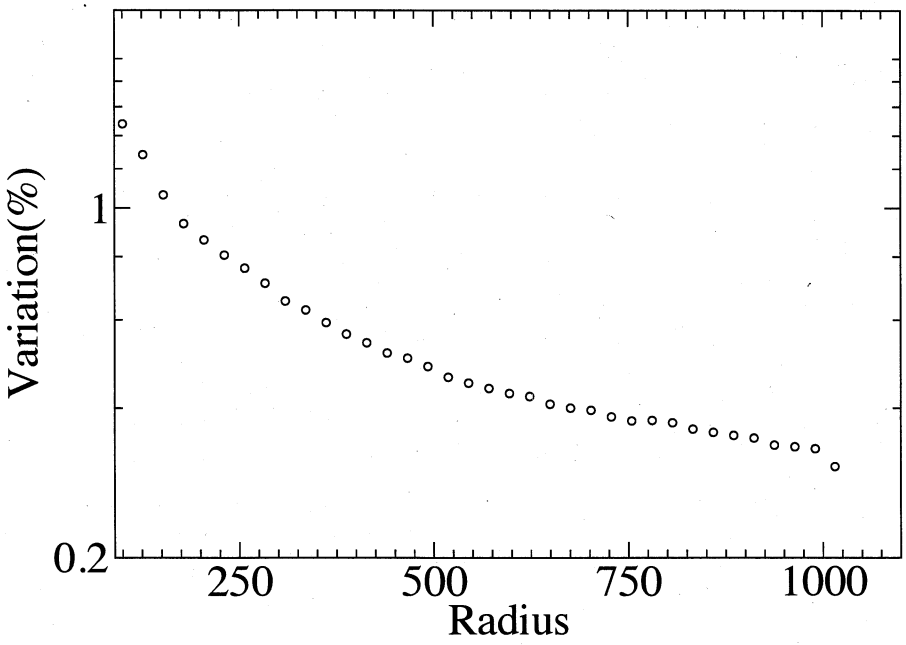

Figure 10: The relationship between the radius of the ring and the variation of the radius.

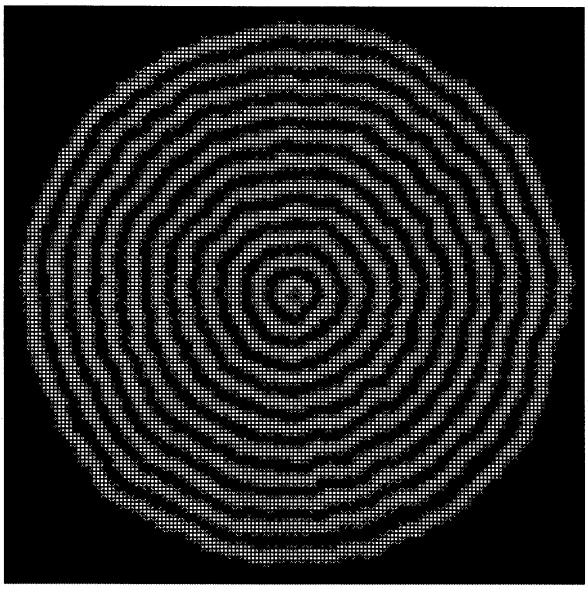

Figure 11: Target pattern. 150×150 cells, $t = 128$, $N = 4$, $\Delta_1 = 3$, $\Delta_2 = 6$, $p = 1/2$.

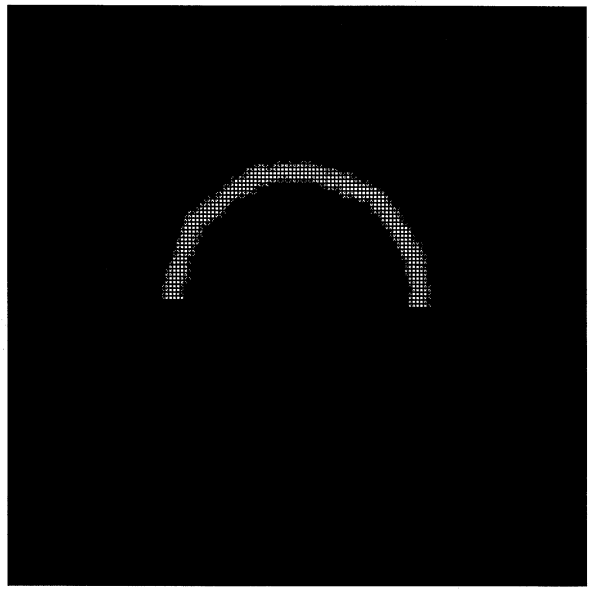

(a)

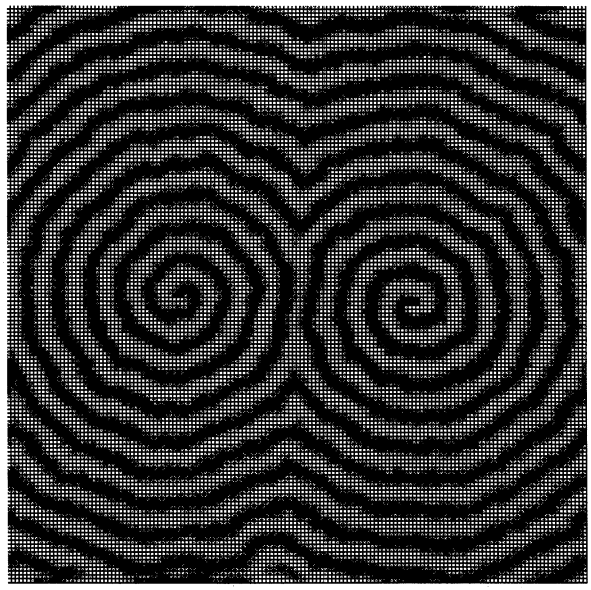

(b)

Figure 12: (a) A cut ring pattern. 150×150 cells, $t = 70$, $N = 5$, $\Delta_1 = 3$, $\Delta_2 = 7$, $p = 1/2$. (b) Spiral pattern. 150×150 cells, $t = 187$, $N = 5$, $\Delta_1 = 3$, $\Delta_2 = 7$, $p = 1/2$.

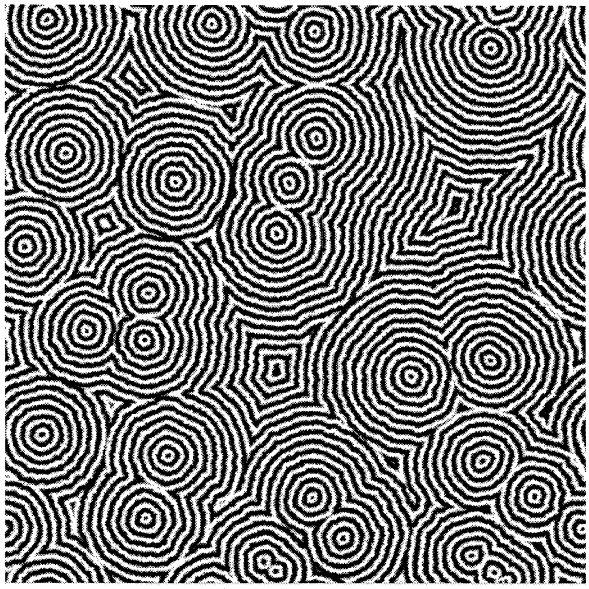

Figure 13: A number of target patterns generated from a random initial condition for 500×500 cells, $t = 304$, $N = 4$, $\Delta_1 = 3$, $\Delta_2 = 6$, $p = 1/2$.

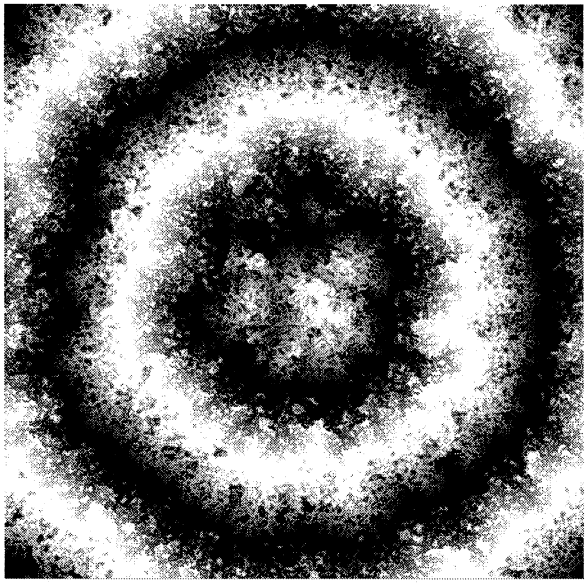

Figure 14: Target pattern in case of a huge number of state values for 400×400 cells, $t = 2952$, $N = 200$, $\Delta_1 = 10$, $\Delta_2 = 400$, $p = 1/2$.

3 General method to construct the isotropic cellular automaton for reaction- diffusion system

In the present chapter, we propose a new method to construct a CA model corresponding to a reaction-diffusion system. The method is based on the random walk and on the phase diagram of reaction equations. We require the method to satisfy the following two conditions: (i)The time evolution pattern of the CA preserves the isotropy of the reaction-diffusion equation. (ii)The CA model explicitly contains the control parameters corresponding to the reaction terms and diffusion terms in the reaction-diffusion equation.

3.1 Methodology

In this section, a method to construct the CA corresponding to a given reaction-diffusion equation is introduced. The idea is very simple: to replace the diffusion term by a random walk process and the reaction terms by time evolution along a discrete vector field obtained from the phase diagram. First, we explain the reaction-diffusion equation in brief, then we introduce our CA model.

3.1.1 Reaction-diffusion equation

Suppose that there are N different reactive materials $U_1, U_2, \cdots, U_N$ in some spatial region. Let the densities of these materials at position $\boldsymbol{r}$ and time t be $u_1(\boldsymbol{r}, t)$, $u_2(\boldsymbol{r}, t)$, $\cdots$, $u_N(\boldsymbol{r}, t)$ respectively, and put $\boldsymbol{u} := (u_1, u_2, \cdots, u_N)^T \in \mathbf{R}^N$. The reaction-diffusion equation is given as

$$\frac{\partial \boldsymbol{u}}{\partial t} = \boldsymbol{f}(\boldsymbol{u}) + D\nabla^2 \boldsymbol{u}, \tag{3}$$

where $D = \mathrm{diag}(d_1, d_2, \cdots, d_N)$ i.e. D is a $N \times N$ diagonal matrix which has the diffusion coefficient d_j for each material as a diagonal element. The vector $\boldsymbol{f}(\boldsymbol{u}) = (f_1(\boldsymbol{u}), f_2(\boldsymbol{u}), \cdots, f_N(\boldsymbol{u}))^T$ expresses the interactions between the materials and $\nabla := \frac{\partial}{\partial \boldsymbol{r}}$ is the nabla symbol, in particular $\nabla^2 = \frac{\partial^2}{\partial x^2} + \frac{\partial^2}{\partial y^2}$ in two spatial dimension: $\boldsymbol{r} = (x, y)$.

3.1.2 The CA model

We now introduce our cellular automaton model for the reaction-diffusion equation (3). For simplicity, we assume that the equation is defined in two spatial dimensions and that the CA model is defined on a two dimensional square lattice. Generalisation to higher dimensional systems and different types of lattices will be straightforward. In the reaction-diffusion equation (3), the variable $\boldsymbol{u}$ represents the density of reactive material. In our CA model, we replace the density of material $\boldsymbol{u}(\boldsymbol{r}, t)$ by the number of microscopic particles $\boldsymbol{u}^t_{mn} \in {\mathbb{Z}_+}^N$ at the corresponding lattice point $(m, n) \in \mathbb{Z}^2$ at time step $t \in \mathbb{Z}/2$. Then the time evolution of our CA model is determined by

$$\begin{aligned} \boldsymbol{u}^{t+1/2}_{mn} &= \boldsymbol{u}^t_{mn} + \boldsymbol{R}(\hat{\boldsymbol{u}}^t_{mn}), \\ \boldsymbol{u}^{t+1}_{mn} &= \boldsymbol{u}^{t+1/2}_{mn} + \boldsymbol{F}(\boldsymbol{u}^{t+1/2}_{mn}), \end{aligned} \tag{4}$$

where $\hat{\boldsymbol{u}}^t_{mn}$ denotes a set of concentration variables around (m, n) at time step t, $\boldsymbol{R}(\hat{\boldsymbol{u}}^t_{mn})$ and $\boldsymbol{F}(\boldsymbol{u}^t_{mn})$ denote discrete vector fields which are obtained by replacing the diffusion and reaction terms of the reaction-diffusion equation respectively with the following processes:

(i) The diffusion term $D\nabla^2\boldsymbol{u}$ corresponds to a random walk of particles. Let us consider a random walk of particles defined in the Neumann neighbourhood $\hat{\boldsymbol{u}}^t_{mn} = \{\boldsymbol{u}^t_{m,n}, \boldsymbol{u}^t_{m-1,n}, \boldsymbol{u}^t_{m+1,n}, \boldsymbol{u}^t_{m,n-1}, \boldsymbol{u}^t_{m,n+1}\}$. One can equally adopt the Moor neighbourhood or other neighbourhoods. We denote by $\boldsymbol{U}^{\rightarrow t}_{mn}$ the stochastic variable which defines the number of particles moving from the (m, n) site to the $(m+1, n)$ site due to the random walk of the particles, by $\boldsymbol{U}^{\rightarrow t}_{m-1,n}$ that from from $(m-1, n)$ to (m, n), and so on. Then $\boldsymbol{R}(\hat{\boldsymbol{u}}^t_{mn})$ equals the difference between the number of outgoing particles and that of the incoming particles due to the random walk at position (m, n) and time t:

$$\begin{aligned} \boldsymbol{R}(\hat{\boldsymbol{u}}^t_{mn}) = \boldsymbol{U}^{\rightarrow t}_{m-1,n} + \boldsymbol{U}^{\leftarrow t}_{m+1,n} + \boldsymbol{U}^{\uparrow t}_{m,n-1} + \boldsymbol{U}^{\downarrow t}_{m,n+1} \\ -(\boldsymbol{U}^{\rightarrow t}_{mn} + \boldsymbol{U}^{\leftarrow t}_{mn} + \boldsymbol{U}^{\uparrow t}_{mn} + \boldsymbol{U}^{\downarrow t}_{mn}). \end{aligned} \tag{5}$$

If we define p_j as the transition probability of particles to one neighbouring cell in the random walk, $1 - 4p_j$ is the probability of particles to stay on site and the expectation of $\boldsymbol{U}^{\rightarrow t}_{mn}$, $\boldsymbol{U}^{\rightarrow t}_{m-1,n}$ etc. are given respectively by $\langle \boldsymbol{U}^{\rightarrow t}_{m,n} \rangle = P\boldsymbol{u}^t_{m-1,n}$, $\langle \boldsymbol{U}^{\rightarrow t}_{m-1,n} \rangle = P\boldsymbol{u}^t_{m-1,n}$ with a diagonal matrix $P = \mathrm{diag}(p_1, p_2, \cdots, p_N)$. We can see that P corresponds to the diffusion coefficient D of the reaction-diffusion equation.

(ii) The reaction term $\boldsymbol{f}(\boldsymbol{u})$ is replaced with an appropriate discrete function $\boldsymbol{F}(\boldsymbol{u}_{mn}^t) = (F_1(\boldsymbol{u}_{mn}^t), F_2(\boldsymbol{u}_{mn}^t), \cdots, F_N(\boldsymbol{u}_{mn}^t))^T \in \mathbb{Z}^N$. In equation (3), the reaction term $\boldsymbol{f}(\boldsymbol{u})$ is the vector field that defines the velocity vector $\frac{\partial \boldsymbol{u}}{\partial t}$. Hence $\boldsymbol{F}(\boldsymbol{x})$ should be so chosen such that the time evolution of $\boldsymbol{x}$ is consistent with the typical orbits in the phase diagram of the ordinary differential equation

$$\frac{d\boldsymbol{u}}{dt} = \boldsymbol{f}(\boldsymbol{u}).$$

Since $\boldsymbol{F}(\boldsymbol{u}_{mn}^t)$ sometimes returns a negative number, it is practically convenient to use the discrete vector field, $\boldsymbol{G}(\boldsymbol{u}_{mn}^t) := \boldsymbol{u}_{mn}^t + \boldsymbol{F}(\boldsymbol{u}_{mn}^t) \geq 0$. Then our CA model is rewritten as

$$\begin{aligned} \boldsymbol{u}_{mn}^{t+1/2} &= \boldsymbol{u}_{mn}^t + \boldsymbol{R}(\hat{\boldsymbol{u}}_{mn}^t), \\ \boldsymbol{u}_{mn}^{t+1} &= \boldsymbol{G}(\boldsymbol{u}_{mn}^{t+1/2}). \end{aligned} \tag{6}$$

We can obtain the time evolution pattern by successive substitution of $\boldsymbol{R}(\hat{\boldsymbol{u}}_{mn}^t)$ and $\boldsymbol{G}(\boldsymbol{u}_{mn}^t)$ for appropriate initial conditions.

It is well known that the continuous limit of the random walk is equivalent to a diffusion equation, and that in the large scale limit, isotropy of the distribution function of the particles is guaranteed by a random walk. Since the discrete vector field $\boldsymbol{F}(\boldsymbol{u})$ is chosen such that it is essentially equivalent to the vector field $\boldsymbol{f}(\boldsymbol{u})$ in the continuous limit, we expect that the patterns obtained from our CA model become almost isotropic in certain large systems. It should be noted that our model naturally contains the parameters $\{p_i\}$ which correspond to the diffusion coefficients and all other control parameters for reactions, which are necessarily contained in the discrete vector field.

3.2 Application to the Belousov-Zhabotinsky reaction

In this section, we apply the method introduced in previous section to the Belousov-Zhabotinsky (BZ) reaction as a specific example. First, we briefly explain the BZ reaction and oregonator known as a mathematical model for this reaction. Next, we introduce our CA model of the BZ reaction.

3.2.1 BZ reaction

Here, we detail the Belousov-Zhabotinsky reaction again. The BZ reaction is known as an oscillating oxidation-reduction reaction which occurs by mixing some chemical

compounds (such as Ce^{4+}, BrO^{3-}, $CH_2(COOH)_2$, H_2SO_4). If the BZ reaction is spread spatially, then it forms trigger waves, spiral waves or target patterns [5]. The BZ reaction is often modeled by using partial differential equations. Among them, the oregonator, which is a system of simultaneous ordinary differential equations with two variables, is widely considered to be the simplest possible model [7]. The time evolution of the spatial patterns in the BZ reaction is described by the following equation which adds diffusion terms to the oregonator:

$$\begin{aligned} \frac{\partial u}{\partial t} &= \frac{1}{\epsilon}\left[u(1-u) - \frac{bv(u-a)}{u+a}\right] + d_u \nabla^2 u, \\ \frac{\partial v}{\partial t} &= u - v + d_v \nabla^2 v, \end{aligned} \tag{7}$$

where b and ϵ (or $1/\epsilon$) are, respectively, a threshold which gives the excitation and a parameter which defines the excitability of reaction respectively. Depending on the parameters a, b and ϵ, Eq. (7) shows two typical states: an excitable state with one stable equilibrium point and an oscillatory state with one unstable equilibrium point. Here we consider only the excitable state (or excitable media).

Let $f(u,v) := \frac{1}{\epsilon}[u(1-u) - \frac{bv(u-a)}{u+a}]$ and $g(u,v) := u - v$. Figure 15 shows the phase diagram for the excitable state of the BZ reaction. The null clines that are obtained from $f(u,v) = g(u,v) = 0$ are shown by solid lines and a typical orbit for the excitable state is shown by a dashed line. The intersecting point of $f = 0$ and $g = 0$ is a stable point if there is no diffusion, however it becomes unstable when the strength of the perturbation (mainly due to the diffusion effects) exceeds a certain threshold δ. Then the state of the medium becomes unstable and changes along the dashed line shown in the phase diagram, until it returns to the equilibrium point once again. The repetition of this process induces spacial patterns such as spiral waves.

3.2.2 The CA model

Our CA model for Eq. (7) is described in the form of Eq. (6), introduced in section 3.1.2. According to Eq. (7), we put $\boldsymbol{u}^t_{mn} := (u^t_{mn}, v^t_{mn})^T$, $\boldsymbol{G}(\boldsymbol{u}^t_{mn}) := (G_u(\boldsymbol{u}^t_{mn}), G_v(\boldsymbol{u}^t_{mn}))^T$ and $\boldsymbol{R}(\hat{\boldsymbol{u}}^t_{mn}) := (R_u(\hat{u}^t_{mn}), R_v(\hat{v}^t_{mn}))^T$.

First, we define the discrete vector field $\boldsymbol{G}(\boldsymbol{u}^t_{mn})$ by imitating the solution orbit of the phase diagram shown in Figure 15. The discrete vector field we configured is shown in Table 2 and illustrated in Figure 16. We can see that Figure 16 is a simplification of the phase diagram of Figure 15. Let $u^t_{mn} \in \mathbb{Z}_+$, $v^t_{mn} \in \{0,1\}$ in

this example of an excitable BZ reaction. Parameters α, β and γ control the rate of reaction, and Δ is the threshold which determines whether the excitation occurs or not. Parameter $N \in \mathbb{Z}_+$ denotes the expected maximum value of variable u^t_{mn}. All of these five parameters are positive integers.

The value of the discrete vector field $\boldsymbol{G}(u^t_{mn}, v^t_{mn})$ is determined in function of the values of u^t_{mn} and v^t_{mn}, as shown in Table 2. For $0 \leq u^t_{mn} < \Delta, v^t_{mn} = 0$, the state of the medium returns to the equilibrium point with velocity α, because the state cannot exceed the threshold Δ due to inadequate diffusion effects. For $\Delta \leq u^t_{mn} < N - 1 - \beta, v^t_{mn} = 0$, the variable u^t_{mn} increases at the rate β until $u^t_{mn} \geq N - 1 - \beta$. In the range $\gamma < u^t_{mn}, v^t_{mn} = 1$, the variable u^t_{mn} decreases at the rate of γ. In the two remaining ranges, the variable v^t_{mn} changes between 0 and 1. Here we assumed $v^t_{mn} \in \{0, 1\}$, because two states are sufficient to separate the phases, according to the medium, corresponding to the variable v^t_{mn}.

In Eq. (7), the excitation of excitable media is determined by the diffusion of u, i.e., $d_u \gg d_v$. Hence, in this example, we only consider the random walk of the variable u^t_{mn} and we simulate the time evolution by putting $P = \mathrm{diag}(p_u, 0)$.

Consequently, our CA model for the excitable BZ reaction is given as:

$$\begin{aligned} u^{t+1/2}_{mn} &= u^t_{mn} + R_u(\hat{u}^t_{mn}), \\ v^{t+1/2}_{mn} &= v^t_{mn}, \\ u^{t+1}_{mn} &= G_u(\boldsymbol{u}^{t+1/2}_{mn}), \\ v^{t+1}_{mn} &= G_v(\boldsymbol{u}^{t+1/2}_{mn}). \end{aligned} \tag{8}$$

3.2.3 Numerical results

In this section, we show several time evolution patterns obtained from Eq. (8) and discuss the results.

(i) Patterns. The first example is a single trigger wave (Figure 17). It is produced by the initial condition $u^0_{mn} = [h \cdot \exp(-((m - L/2)^2 + (n - L/2)^2)/w^2)]$ and $v^0_{mn} = 0$ on a 2-dimensional square area with $L \times L$ cells. Here $[\,]$ is Gauss' symbol, i.e.: $[x]$ is the largest integer that is less than or equal to x and h and w are positive real numbers. We observed that from a pulse triggered at the center, a ring-shaped wave spreads outwards in an almost isotropic fashion.

In order to generate a spiral wave, appropriate initial conditions are necessary. Firstly, we generate a single trigger wave like the one shown in Figure 17. Then we cut off one part of the ring pattern as shown in Figure 18 (a) and use the remainder

as the initial state. The spiral wave obtained from our model is shown in Figure 18 (b).

The third example is a target pattern (Figure 19). The initial condition is the same as in the case of the trigger wave, but with different parameters. From the central pulse, ring-shaped waves are produced repeatedly.

(ii) Anisotropy. We evaluate the anisotropy of the trigger wave in Figure 17 by measuring the residual error when compared with the average radius of the ring, and plot it in Figure 20 as a function of the propagation direction. We find that the wave fronts of the trigger wave propagate in each direction with an anisotropy in the range of ± 2.5 percent. In Figure 21 we plot the variation from the circle as a function of the radius of the trigger wave. It shows that the trigger wave indeed grows closer to a complete circle as the radius (and therefore time) increases.

Next, we evaluate the parameter dependency of the anisotropy for the patterns observed from our model. In Figures 22 and 23, the variations of the wavefronts of trigger waves propagated to radius 450, are plotted as a function of the transition probability p_u of particles by changing parameters β (Fig. 22) and Δ (Fig. 23). We find that the patterns become more isotropic when diffusion becomes stronger, and that they tend to be isotropic for smaller β, but depend less on Δ.

(iii) Parameters. Our CA model has six parameters N, p_u, Δ, α, β and γ. The parameter Δ corresponds to b in Eq. (7) and defines the threshold of excitation; β corresponds to $1/\epsilon$ which defines the excitability of reaction. Figure 24 is the phase diagram of our model obtained by changing the values of Δ and β. The remaining parameters are chosen as $N = 50$, $p_u = 0.1$,$\alpha = \gamma = 1$. We confirm that spiral waves can be generated in a wide region of the parameters. In an even larger parameter range, we find there exist three different regions; one without propagating waves, one allowing for trigger waves (or broken trigger waves), and one chaotic pattern region.

The parameter range for the spiral waves obtained from Eq. (7) has been examined in detail by Jahnke and Winfree [8]. The general tendency is that, when b is sufficiently large, the spiral wave does not appear and for $1/\epsilon \gg 1$ the spiral wave destabilizes and chaotic behaviour is observed. As shown in Figure 24, the phase diagram of our model has the same feature as that for Eq. (7), and we may conclude that the parameters Δ and β play the same role as the control parameters of the reaction terms in the reaction-diffusion equation.

3.3 Summary

We have proposed a method to construct a CA model corresponding to a reaction-diffusion equation, in which the diffusion effect is replaced by a random walk with transition probability matrix P and the reaction by discrete vector fields. The model can include control parameters for both diffusion and reaction, as is the case in the reaction-diffusion equation. As an example, we have shown that our model can successfully reproduce the patterns of BZ reaction. Applications to other reaction-diffusion systems such as FitzHugh-Nagumo equation [33] are interesting future problems. In the present method, however, there are still various candidates for the time evolution rules, depending on the choice of the discrete vector fields that are supposed to have similar features to those of the continuous vector fields, given by the reaction-diffusion equation. Of course we can also adopt discrete vector fields by investigating the reaction process from a microscopic point of view. The determination a suitable time evolution rule will depend on the individual phenomenon and we will investigate this problem extensively in the future.

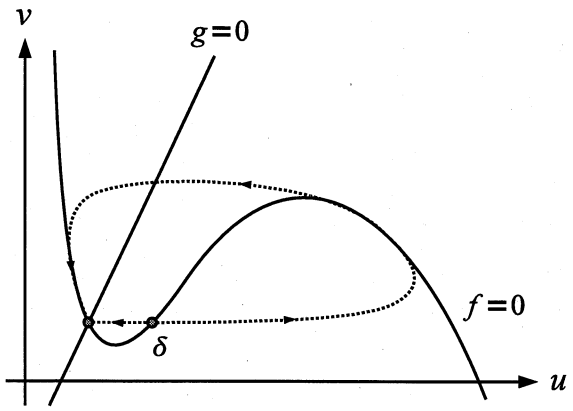

Figure 15: The phase diagram for the excitable BZ reaction.

Table 2: Example of discrete vector field $\boldsymbol{G}(\boldsymbol{u}^t_{mn})$ for an excitable medium.

$(u^t_{mn}, v^t_{mn}) = \boldsymbol{u}^t_{mn}$	$(G_u(\boldsymbol{u}^t_{mn}), G_v(\boldsymbol{u}^t_{mn})) = \boldsymbol{G}(\boldsymbol{u}^t_{mn})$
$(0 \leq u^t_{mn} < \Delta, v^t_{mn} = 0)$	$(\max[u^t_{mn} - \alpha, 0], 0)$
$(\Delta \leq u^t_{mn} < N - 1 - \beta, v^t_{mn} = 0)$	$(u^t_{mn} + \beta, 0)$
$(N - 1 - \beta \leq u^t_{mn}, v^t_{mn} = 0)$	$(N - 1, 1)$
$(\gamma < u^t_{mn}, v^t_{mn} = 1)$	$(u^t_{mn} - \gamma, 1)$
$(0 \leq u^t_{mn} \leq \gamma, v^t_{mn} = 1)$	$(0, 0)$

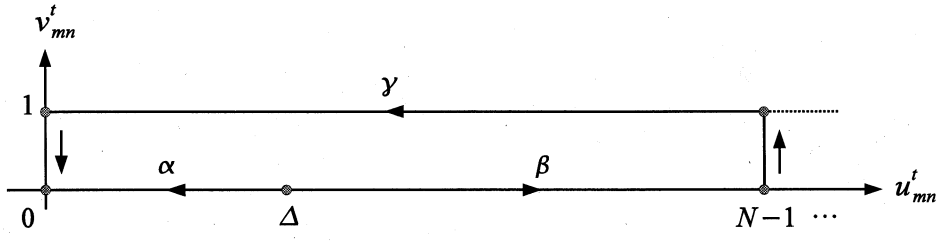

Figure 16: Outline of the discrete vector field $\boldsymbol{G}(\boldsymbol{u}^t_{mn})$ in Table2.

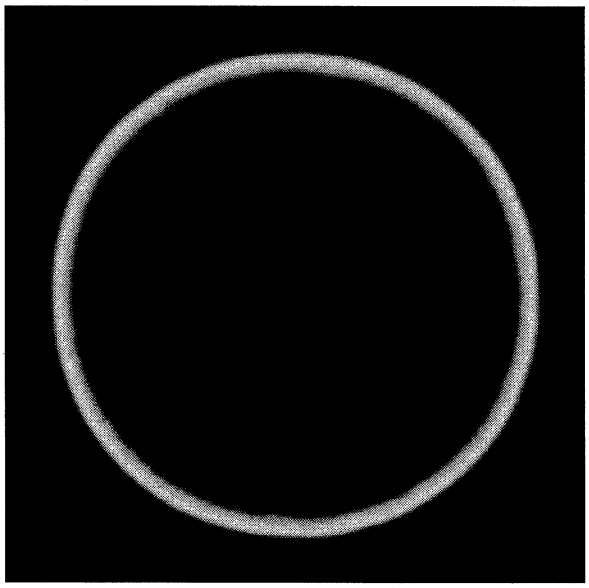

Figure 17: Single trigger wave. 500×500 cells, $t = 5850$, $N = 100$, $p_u = 0.2$, $\Delta = 21$, $\alpha = 1$, $\beta = 1$, $\gamma = 1$.

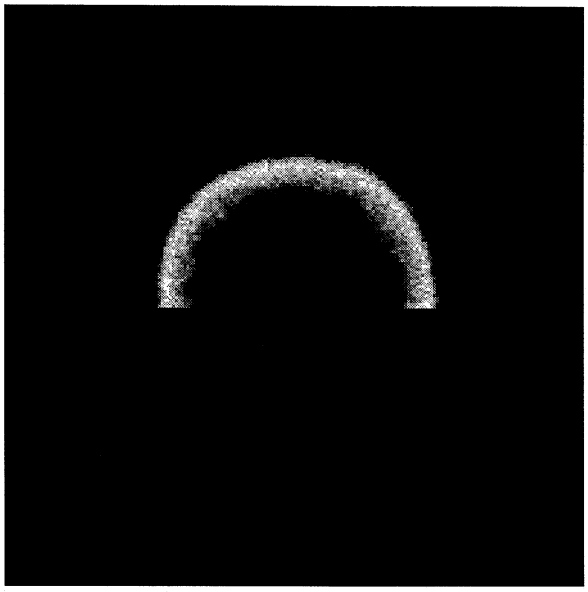

(a)

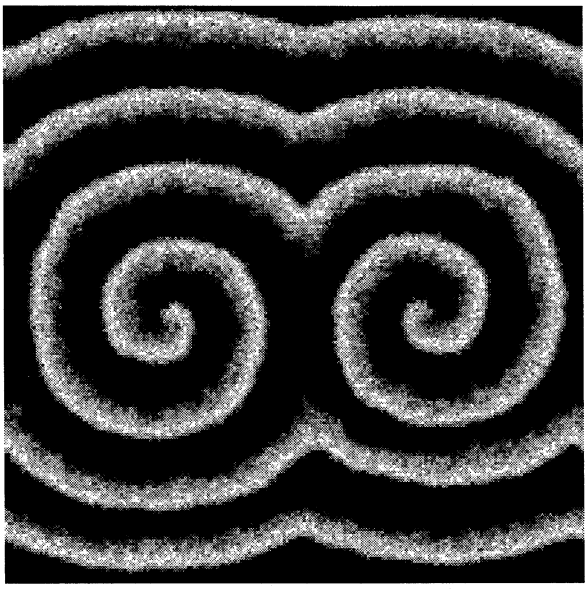

(b)

Figure 18: (a) A cut trigger wave. 200×200 cells, $t = 250$, $N = 30$, $p_u = 0.2$, $\Delta = 6$, $\alpha = 1$, $\beta = 2$, $\gamma = 1$. (b) Spiral wave. 200×200 cells, $t = 963$, $N = 30$, $p_u = 0.2$, $\Delta = 6$, $\alpha = 1$, $\beta = 2$, $\gamma = 1$.

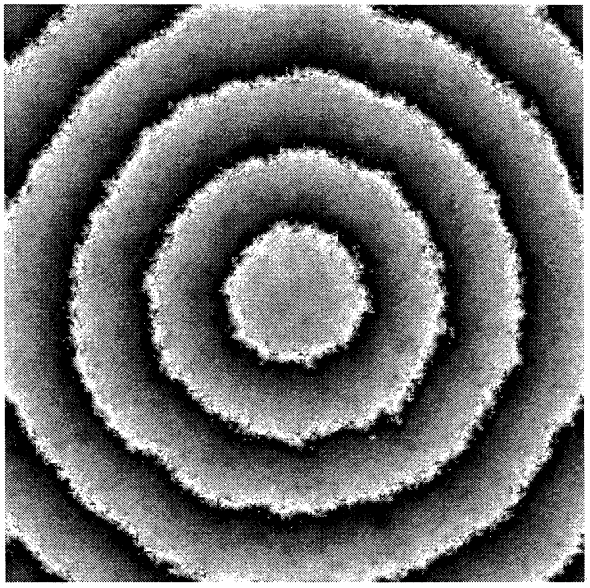

Figure 19: Target pattern. 300×300 cells, $t = 626$, $N = 100$, $p_u = 0.04$, $\Delta = 2$, $\alpha = 1$, $\beta = 10$, $\gamma = 1$.

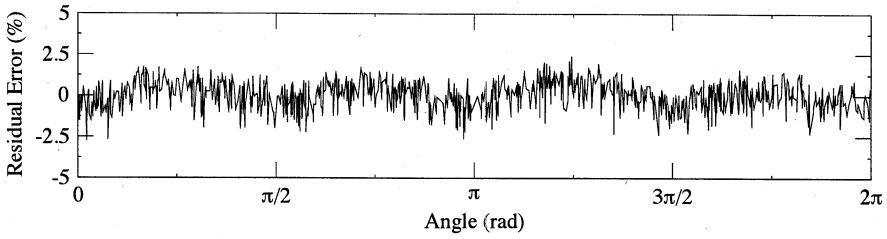

Figure 20: Plot of the anisotropy of the model, measured as the residual error of the trigger pattern in Figure17.

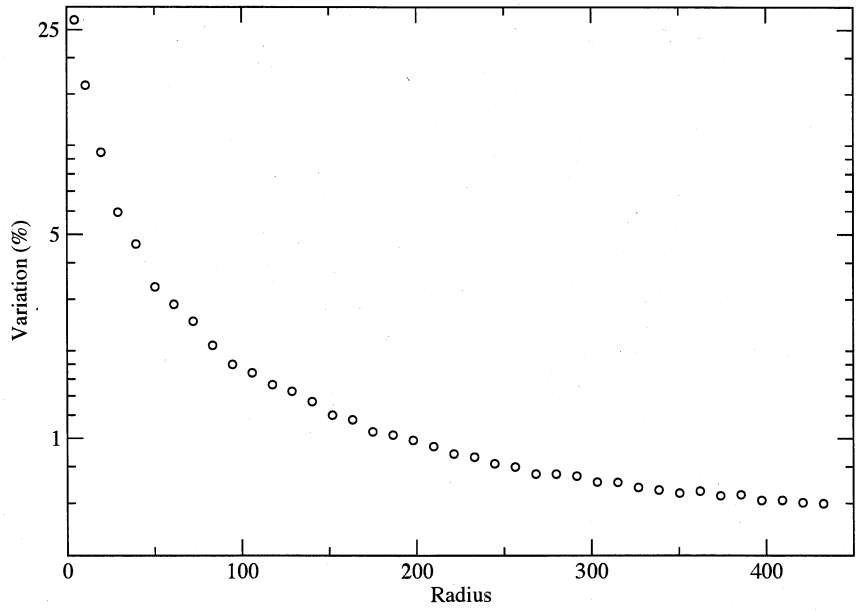

Figure 21: The relationship between the radius of the ring and the variation of the radius.

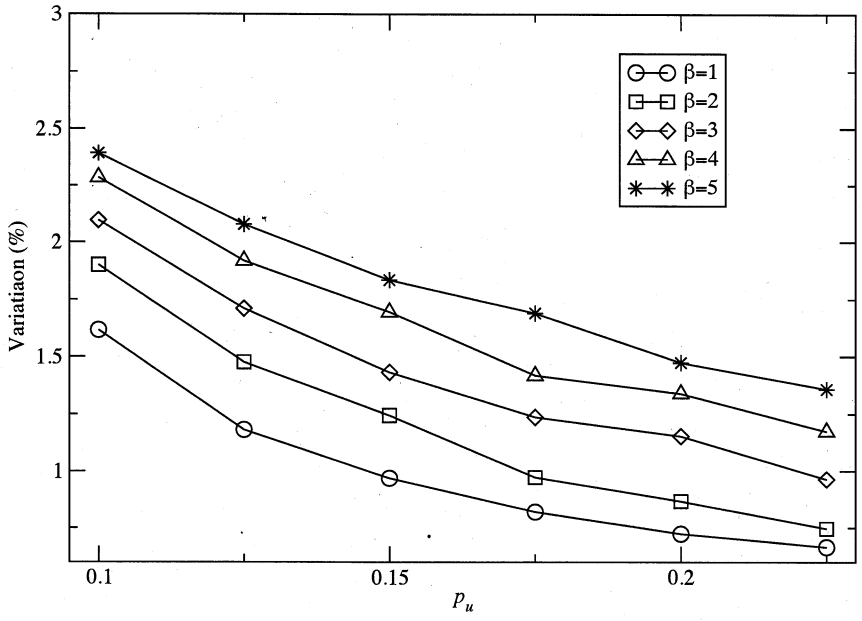

Figure 22: The parametric dependency of the anisotropy of the model for the parameter β. $N = 100$, $\Delta = 15$, $\alpha = 1$, $\gamma = 1$.

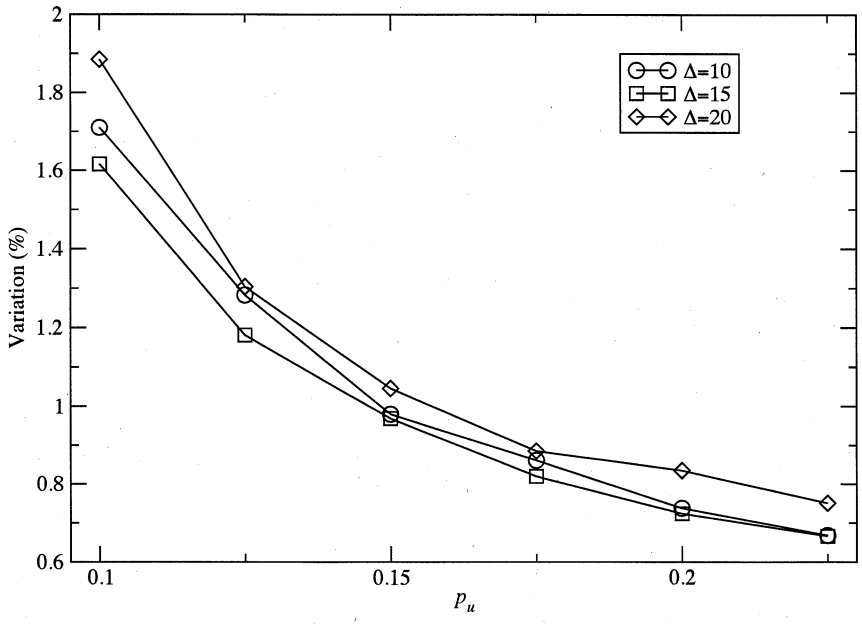

Figure 23: The parameter dependence of the anisotropy of the model on the parameter Δ. $N = 100$, $\alpha = 1$, $\beta = 1$, $\gamma = 1$.

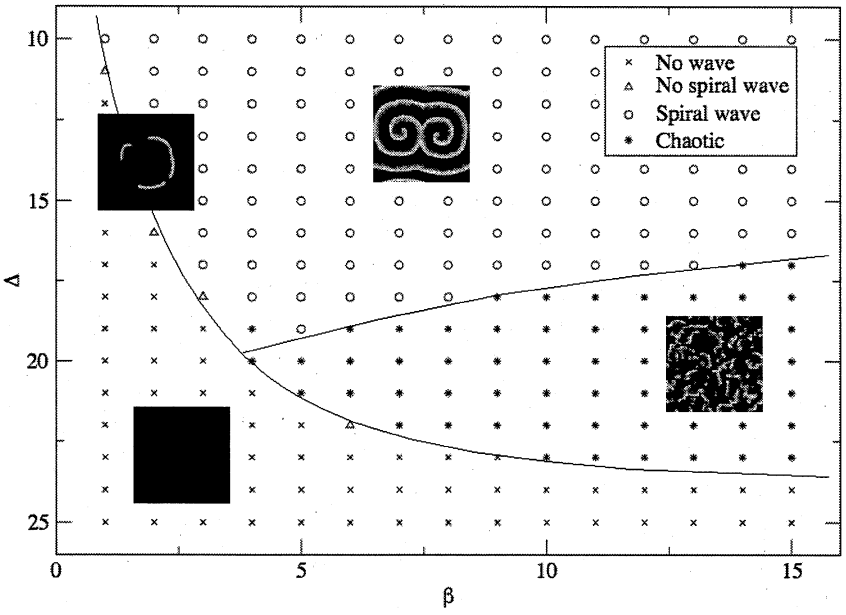

Figure 24: The phase diagram of the patterns obtained from our CA. $N = 50$, $p_u = 0.1$, $\alpha = \gamma = 1$.

4 Application to the growth model of bacterial colonies

In the present chapter, we apply the method introduced in previous chapter to the growth patterns of bacterial colonies.

4.1 Modelling of bacterial colonies

Modelling the patterns observed in bacterial colonies is one of the most interesting applications of a physical approach to biological systems. Colonies of migrating bacteria are characterised by a great variety of behaviour. The latter manifests itself through the patterns that the colony exhibits during their spatio-temporal evolution and which can be observed and studied at a macroscopic level. The particular interest, from a physical point of view, of migrating bacteria is that they can be analysed as systems the collective behaviour of which is controlled by a moderate number of parameters. This makes possible to set up and conduct experiments where all the important parameters are precisely controlled, leading to results which can be most useful in the construction of models.

Two different approaches can be (and have been) used for the morphological description of bacterial colonies. The first is an approach based on differential systems [36, 39, 40, 44, 45, 46, 51, 47, 52, 42] (for thorough reviews one can consult [37, 48]). This continuous approach has the definite advantage of familiarity. The mathematical models which encode the laws of physics are cast in differential form and thus the abecedary of modelling is comprised in large part of differential systems. However, the use of a differential formulation is usually associated with the introduction of a macroscopic description of the system where one follows the evolution of a few collective variables. This is a mixed blessing. While the macroscopic approach condenses the information into a few, hopefully pertinent and in any case easy to follow, parameters, it may sometimes lead to over-simplifications and an inadequate description of the dynamics of the system. At the antipodes of the continuous lies the "discrete" formulation of the model. It is usually associated with a fully microscopic description of the system where the basic dynamical entities are the objects (represented by their physical properties) the dynamics of which one intends to model. The advantage of the discrete approach is that it offers a clear visual representation of the situation. To borrow an example from the domain in

which this chapter is situated, in a discrete model of migrating bacterial colonies the elementary objects are the bacteria (or a group of them) represented through their positions and the model consists in a set of rules for their temporal evolution [38, 26]. The main disadvantage of discrete models compared to continuous ones is in fact the profusion of information. When the discrete model is not a deterministic but a stochastic one, as is often the case, the plethora of information is tainted by the fluctuations due to the random character of the evolution and the initial data. It becomes then mandatory to prune the meaningless details and extract the meaningful information, a task that may sometimes prove quite arduous.

Discrete models and more specifically those aiming at the description of migration (be it of bacteria or other elementary entities such as migrating tumour cells) are often based on cellular automata [34, 35, 26]. The advantage of the latter is that it offers a natural spatial representation of the situation in particular when each cell of the automaton represents a single bacterium (or a group of them). The derivation of a cellular automaton model for the description of migration may proceed in two different ways. The first is an ab initio construction where one must choose the geometry and the rules of the automaton (using also a dose of intuition). In the second approach the automaton is essentially a convenient tool for performing the simulation. Here one starts from a continuous model and introduces an appropriate discretisation. For instance, if one considers that the collective motion of migrating bacteria can, during certain phases of the process, be described by a diffusion equation, the corresponding cellular automaton could consists either in a set of random-walk-type rules (in the ab initio construction) or in an effective discretisation of the diffusion equation. The ab initio approach presents the advantage that one can choose freely the geometry of the automaton. In a studies by Badoual et al. [26] it was shown that a Voronoi tessellation constructed on a set of points obtained from the (small) random deformation of a triangular lattice is quite adequate for the simulation of the dynamics of migrating bacterial colonies. On the other hand the approach based on the discretisation of a continuous system does present a certain difficulty. As a matter of fact the discretisation of a partial differential equation is straightforward when performed on a regular lattice. The drawback of this approach is that a regular lattice breaks the isotropy of space and introduces privileged directions of propagation. Fortunately this can be remedied in a simple way. As shown in chapter 2 it is possible, through the introduction of a simple probabilistic rule among neighbouring cells to obtain isotropic time-evolution patterns in a cellular

automaton based on a square lattice [21].

The present chapter is devoted to the modelling of migrating colonies of the bacteria *Bacillus subtilis* and *Proteus mirabilis*. The acid test of the validity of the model is to reproduce the morphological diagrams of both species ([49, 41, 56, 61] for *Bacillus subtilis* and [53, 64] for *Proteus mirabilis*). Despite a different detailed biological behaviour, we can reasonably assume that the physical principles are the same for *Bacillus subtilis* and *Proteus mirabilis*, a view supported also by the statement of Yamazaki et al: "We expect that there exists a universal mechanism of the bacterial colony growth into concentric ring pattern irrespective of bacterial species" [64]. Once this is established we proceed to the modelling of subtler properties experimentally investigated in a recent study of the team of Chuo University, well-known for its pioneering studies on bacterial colonies. We show that, with reasonable assumptions, it is possible with our simple model to reproduce the experimental findings.

4.2 The CA model

In order to model the time evolution of the bacterial colony we have chosen a cellular automaton model. The geometry of the automaton is a two-dimensional square lattice. The use of a regular lattice usually results to artificially anisotropic patterns necessitating the use of a very small lattice step and huge domains in order to attain some semblance of isotropy. In order to remedy this one can use a non-regular lattice, for instance a Voronoi lattice resulting from a Delaunay triangulation [25], used already by Badoual et al. in the modelling of bacterial colonies [26]. However as shown in previous chapter there exists an alternative approach [54]. It is indeed possible, by introducing the adequate randomness in the rules defining the discrete diffusion process, to obtain an isotropic cellular automaton model over a regular lattice. This is the approach we shall follow in this chapter.

We start by introducing two populations of bacteria, active and inactive, the related variables being $b^t_{i,j}$ and $s^t_{i,j}$. Here (i, j) correspond to the lattice points, while t is the time variable (given in discrete time steps). Moreover we introduce a variable $n^t_{i,j}$ corresponding to the quantity of nutrients (in arbitrary units). (We remind here that since we are dealing with a cellular automaton all the variables take integer values).

The time evolution of our automaton can be schematically expressed as

$$u_{i,j}^{t+1/2} = u_{i,j}^{t} + R(\tilde{u}_{i,j}^{t}, p_u) \tag{9a}$$

$$u_{i,j}^{t+1} = F(u_{i,j}^{t+1/2}) \tag{9b}$$

The variable u stands for the triplet b, s, n. The tilde in $\tilde{u}_{i,j}^{t}$ indicates a set of variables in the immediate vicinity of (i, j). The two equations model the two phases of the evolution i.e. migration (through a diffusion process) for (9a) and consolidation for (9b). During the migration phase the active bacteria, as well as the nutrients, perform a random walk in their neighbourhood, encoded by R, with transition probability p_u. During the consolidation phase the number of active and inactive bacteria and the quantity of nutrient increase or decrease due to local nonlinear interactions (represented by F). Two variants of the model should be distinguished at this point. The first corresponds to a nutrient-poor case where the effect of the nutrient scarcity plays a crucial role. The second corresponds to a nutrient-rich case. Here the variations of the quantity of nutrient are not playing any role and thus we simplify the model by ignoring the evolution of n altogether. We have thus:

4.2.1 Model A

In this model, we introduce three integer parameters Δ_{Low}, Δ_{High} and Δ_n ($\Delta_{Low} < \Delta_{High}$) as threshold values for the evolution, and two parameters p_b and p_n which are the transition probabilities of the random walk for the variables $b_{i,j}^{t}$ and $n_{i,j}^{t}$ respectively. The random walk is defined in a neighbourhood comprising the "particle" represented by u and its four nearest neighbours on the two-dimensional square lattice. Thus $R(\tilde{u}_{i,j}^{t})$ is equal to the difference between the number of outgoing and incoming particles due to the random motion at position (i, j) and time t. Then the time evolution rule is defined by the following two steps:

(i) The migration phase

If $\Delta_{Low} < b_{i,j}^{t}$, then

$$b_{i,j}^{t+1/2} = b_{i,j}^{t} + R(\tilde{b}_{i,j}^{t}, p_b)$$

$$n_{i,j}^{t+1/2} = n_{i,j}^{t} + R(\tilde{n}_{i,j}^{t}, p_n)$$

$$s_{i,j}^{t+1/2} = s_{i,j}^{t}$$

Otherwise,

$$b_{i,j}^{t+1/2} = b_{i,j}^{t}$$

$$n_{i,j}^{t+1/2} = n_{i,j}^{t} + R(\tilde{n}_{i,j}^{t}, p_n)$$
$$s_{i,j}^{t+1/2} = s_{i,j}^{t}$$

Here the random walk for the variable $b_{i,j}^t$ is not uniform, but is directed in the sense that the bacteria are allowed to move only to a site with lower number of neighbours compared to those of the site on which the are.

(ii) The consolidation phase

If $\Delta_n < n_{i,j}^t$ and $b_{i,j}^{t+1/2} + s_{i,j}^t < \Delta_{High}$, then

$$b_{i,j}^{t+1} = \max[b_{i,j}^{t+1/2} + \alpha b_{i,j}^{t+1/2} - \beta b_{i,j}^{t+1/2}, 0]$$
$$n_{i,j}^{t+1} = \max[n_{i,j}^{t+1/2} - \gamma b_{i,j}^{t+1/2}, 0]$$
$$s_{i,j}^{t+1} = s_{i,j}^{t+1/2} + \beta b_{i,j}^{t+1/2}$$

or, if $\Delta_n < n_{i,j}^t$ and $b_{i,j}^{t+1/2} + s_{i,j}^{t+1/2} \geq \Delta_{High}$, then

$$b_{i,j}^{t+1} = \max[b_{i,j}^{t+1/2} - \beta b_{i,j}^{t+1/2}, 0]$$
$$n_{i,j}^{t+1} = \max[n_{i,j}^{t+1/2} - \gamma b_{i,j}^{t+1/2}, 0]$$
$$s_{i,j}^{t+1} = s_{i,j}^{t+1/2} + \beta b_{i,j}^{t+1/2}$$

Otherwise,

$$b_{i,j}^{t+1} = \max[b_{i,j}^{t+1/2} - \beta b_{i,j}^{t+1/2} - \lambda b_{i,j}^{t+1/2}, 0]$$
$$n_{i,j}^{t+1} = \max[n_{i,j}^{t+1/2} - \gamma b_{i,j}^{t+1/2}, 0]$$
$$s_{i,j}^{t+1} = s_{i,j}^{t+1/2} + \beta b_{i,j}^{t+1/2} + \lambda b_{i,j}^{t+1/2}$$

Here αb is a random variable which takes an integer value n_b $(0 \leq n_b \leq b)$ with probability $\frac{b!}{n_b!(b-n_b)!}\alpha^{n_b}(1-\alpha)^{b-n_b}$ $(0 \leq \alpha \leq 1)$, the random variables βb, γb and λb being similarly defined. The coefficients α, β, γ, and λ are the proliferation rate of active bacteria, the conversion rate from active to inactive bacteria, the consumption rate of nutrients and the conversion rate to inactive bacteria due to starvation of active bacteria, respectively.

4.2.2 Model B

As explained above the variable n is neglected here since the initial quantity is large enough for variations to have a negligible effect on the colony. Here we introduce a transition probability $p_{i,j}^t \in \{p_{Low}, p_{High}\}$, where $0 \leq p_{Low} \ll 1$ and $p_{Low} < p_{High} \leq 0.25$. The time evolution rule is defined by the following two steps:

(i) The migration phase

If $\Delta_{Low} < b_{i,j}^t$, then

$$b_{i,j}^{t+1/2} = b_{i,j}^t + R(\tilde{b}_{i,j}^t, p_{i,j}^t)$$
$$s_{i,j}^{t+1/2} = s_{i,j}^t$$

Otherwise,

$$b_{i,j}^{t+1/2} = b_{i,j}^t$$
$$s_{i,j}^{t+1/2} = s_{i,j}^t$$

Here, the random walk for the variable $b_{i,j}^t$ is a directed random walk as in Model A.

(ii) The consolidation phase

If $\Delta_{Low} < b_{i,j}^{t+1/2}$ and $b_{i,j}^{t+1/2} + s_{i,j}^{t+1/2} < \Delta_{High}$ and $0 \leq b_{i,j}^{t+1/2} - b_{i,j}^{t-1/2}$, then

$$b_{i,j}^{t+1} = \max[b_{i,j}^{t+1/2} + \alpha b_{i,j}^{t+1/2} - \beta b_{i,j}^{t+1/2}, 0]$$
$$s_{i,j}^{t+1} = s_{i,j}^{t+1/2} + \beta b_{i,j}^{t+1/2}$$
$$p_{i,j}^{t+1} = p_{Low}$$

Otherwise,

$$b_{i,j}^{t+1} = \max[b_{i,j}^{t+1/2} - \beta b_{i,j}^{t+1/2}, 0]$$
$$s_{i,j}^{t+1} = s_{i,j}^{t+1/2} + \beta b_{i,j}^{t+1/2}$$
$$p_{i,j}^{t+1} = p_{High}$$

As in Model A, the coefficients α and β are the proliferation rate of active bacteria and the conversion rate from active to inactive bacteria respectively.

4.3 The morphological diagrams

In what follows we shall present results of the application of our model to the description of patterns observed in migrating colonies of the bacteria *Proteus mirabilis* and *Bacillus subtilis*. The first species of bacteria has a very simple morphological pattern [53, 64] . When one inoculates a seed on an agar plate the colony grows through successive consolidation and swarming phases forming always (at least over a wide range of substrate hardness and nutrient concentration) concentric circles (which materialise a locally higher density of bacteria). The effect of agar concentration, which regulates the substrate hardness, is to lead to circles that are packed more and more tightly as the substrate becomes harder. Thus the morphology of colonies of *Proteus mirabilis* is rather simple. Moreover, as explained in [57, 63], the effect of nutrient availability on the colony aspect is insignificant (although it does have a major effect on the total biomass of the colony).

The situation concerning *Bacillus subtilis* is quite different. The colonies of the latter exhibit a particularly rich behaviour [49, 41, 56, 61] . This situation is best represented through the morphological diagram for this bacterium. The diagram, given in figure 25, delimits the various regions where specific forms of the bacterial colony are encountered, as a function of substrate hardness and nutrient availability. It must be stressed here that the regions are separated by zones of crossover where the shapes go smoothly from one form to the next one [55] (note that the region C can have a slightly different shape in other publications [41, 56, 61]). Two main areas should be distinguished in the morphological diagram, the ones with nutrient abundance and the ones under nutrient scarcity. In the latter we observe always a branch-like organisation of the colony due to the fact that the bacteria are always seeking regions where the nutrient is not yet depleted. When the agar concentration is large (hard substrate) the branches are short and thick, since the colony expands very slowly. This is represented in the zone A of the morphological diagram. When the substrate becomes softer the branches become longer and thinner and eventually we obtain the situation of zone E. The upper part of the morphological diagram corresponds to the nutrient rich situation. Here the behaviour of the colony is essentially dictated by the hardness of the substrate. Thus when the agar concentration is very large the colony is compact: it grows essentially through proliferation (zone B). On the contrary, when the substrate is very soft (zone D) the colony is dilute and isotropic with a very low density. The interesting

feature is the one encountered in zone C, of intermediate substrate hardness. There the migration and consolidation phases are in competition and they result in a ring-like structure of the colony. The reproduction of this special structure is a particular challenge in modelling approaches.

We start with the results on *Proteus mirabilis*. In figure 26a,b,c we show three characteristic ring structures obtained for parameters of the model which are meant to model a substrate becoming progressively softer (from figure c to a). We observe indeed rings that are more and more wide apart as the medium becomes softer leading to a growing colony extension. Figure 26e shows corresponding experimental results [57].

Next we turn to the case of *Bacillus subtilis*. Zone A corresponds to figure 27. The branch-like structure is apparent and one can clearly see that the colony grows by tip-splitting of the branches. The growth of this colony is the slowest one. For instance in our model it takes four times longer than the growth of a colony corresponding to region B. Figure 28a shows such a colony. We remark that the frontier of the colony is smooth and does not show the structure which is often referred to as Eden-like. This is something that we can easily reproduce provided we use model A, which lets the nutrient concentration to play some role. We obtain then figure 28b where we notice a richly structured colony frontier. In both cases the growth of the colony is mainly due to the proliferation of bacteria. Zone D, figure 29, on the other hand corresponds to a diffuse colony where the bacteria move very easily due to the softness of the substrate. This is the fastest growing colony (in agreement with experiment). The qualitatively same result is obtained in this case with both models, i.e. whether we take into account the role of the nutrients or we consider them sufficiently abundant. The density profiles corresponding to cases B and D are shown in figure 30. The same facilitated, random-walk-like, movement of bacteria prevails in zone E as well. Figure 31 shows the shape of such a colony. Again, due to nutrient paucity the bacteria move along branches, the tips of which are repeatedly split as the bacteria seek the scarce nutrient. Finally in figure 32 we present a case where ring-like structure are evident. Here the colony grows alternating (fast) migration and (slow) consolidation phases.

We can conclude, based on the results presented just above, that the overall agreement with the experimental data is quite satisfactory and thus the model is quite efficient in reproducing the various experimental situations. It is thus natural to try to confront our model with more detailed experimental results.

4.4 Modelling more detailed experiments

In this section we are going to use our model in order to reproduce experimental results on colonies of *Bacillus subtilis*. We shall focus on the study of the group of Chuo University reported in [58]. Previous studies of the same group on the bacterium *Proteus mirabilis* have led to a series of observations on the mechanisms underlying the migration and growth of colonies. It was thus crucial for the experimentalists to analyse the behaviour of colonies of *Bacillus subtilis* from the same point of view, since the colonies of this species have a far richer morphology than those of *Proteus mirabilis*.

The existence of a concentric circle structure, common in the two species, stems from periodically alternating phases of migration and consolidation [57, 53, 43, 50, 63, 58, 64]. Thus the first question asked by the experimental group is what is the underlying mechanism of this periodicity. External chemical factors, in fact nutrient, which is the only one in any abundance, could not be at the origin of this mechanism since it is known that the amount of nutrient does not have a significant influence on migration and consolidation times [57, 63]. The two hypotheses which were introduced, tested and discarded were those of the existence of a central pacemaker or of an entrainment of biological origin. Two ingenious experiments were devised in order to test these hypotheses. In the first a triangular sector of the colony was removed leaving only a thin outermost crown. The result was that the colony pursued it growth without appreciable modification in the ring structure, confirming thus the absence of a central pacemaker. The second experiment consisted in implanting two colonies at different times in such a way so as to induce a phase difference in the ring formation. When the two expanding colonies came into contact no phase entrainment was observed at the boundary. They concluded that the origin of the periodicity observed was not to be sought in a biological synchronisation.

We have performed two simulations aiming to reproduce these experimental findings. We should make clear from the outset that our model has in-built the hypotheses of absence of central pacemaker and of biological phase entrainment. Thus results similar to the experimental ones should not be surprising. On the contrary had we found something drastically different this would cast doubts upon our model and perhaps even the conclusions of the experimentalists. In figures 33a and 33b we present a simulation were a triangular sector is removed from the colony. We remark that the growth of the colony is not affected by the excision: the ring pattern

does not present any major alterations. Figures 33c and 33d show corresponding experimental results. Figure 34a corresponds to the case of two colliding colonies. A careful examination of the outermost part of the colonies (figure 34b) shows that, despite the fact that they are in contact to the point of having formed common rings, they keep their respective phases and no synchronisation occurs. Figures 34c and 34d show corresponding experimental results.

So what was the conclusion of the Chuo group? In the absence of a either biological or chemical control factors, they concluded that a physical factor was operative, the local density of bacteria. According to this line of reasoning, migration starts when the density of bacteria exceeds some upper threshold and stops when the density falls below a lower threshold, signaling thus the beginning of consolidation. This hypothesis, already explored in the model presented in [26], is the one our model was built upon. It is interesting at this point to show a result obtained in a situation similar to the experimental one where the role of the low-density threshold was investigated. After an evolution of the colony leading to the appearance of a few successive rings we isolate the outermost migrating bacteria from the rest of the colony and let them evolve. Figure 35a,b shows the "cutting" procedure and the result. We observe two close-lying consolidation rings, one at the edge of the cut and one generated by the migrating bacteria. The latter entered a consolidation phase earlier than expected because of the lower local density caused by the cut. Beyond this ring the evolution of the colony proceeds as before and the spacing of the rings becomes normal again.

Once the hypothesis of density as controlling factor was validated (to be fair we should say "not invalidated") the experimental studies concentrated on the details of bacteria migration, based on the method of replica printing. The latter consists in excising a sectorial part of the colony and transferring it onto a fresh agar plate. The behaviour of the implanted colony depends on the time of excision. We can summarise the results thus: when the colony is in early migration phase the bacteria expand from the front of the sector, while when the colony is in early consolidation phase the expansion takes place from the sides of the sector. More detailed analyses suggest that the active bacteria move in the consolidation ring from the inner part and from there to the front of the colony. We have performed the digital analogue of these replica-printing experiments. Figures 36a and 36b show the evolution of a triangular sector where the excision has taken place at early migration phase. We remark that the bacteria expand from the front of the colony. In fact a colony of

circular form with an inner ring structure is obtained situated at the front of the last consolidation terrace. Figures 36c and 36d show corresponding experimental results. The second simulation consists in isolating a triangular sector when the colony is in consolidation phase at three different moments: early, middle and late consolidation phase. The results are shown in figures 37a, 37b and 37c respectively. We remark that when we are in early consolidation phase the expansion is essentially lateral. On the other hand at a late consolidation the expansion is mainly frontal. Quite expectedly a intermediate situation is observed for an excision in middle consolidation phase. Our results are thus compatible with the conclusions of the experimental group. Figures 37d, 37e and 37f show corresponding experimental results. In conclusion our simple model not only reproduces the morphological diagrams of both species but it allows the simulation of more detailed experiments leading in a quite satisfactory agreement with the experimental findings.

4.5 Conclusion and outlook

In this chapter we have addressed the question of the evolution of a colony of bacteria from the point of view of modelling. The model was based on a cellular automaton and was inspired by a method introduced in previous chapter. As was shown in [54] it is possible to simulate diffusion effects through a random walk on a regular lattice without the unphysical anisotropy induced by the lattice regularity. (An alternative method based on a non-regular lattice was equally explored in [26] by Badoual et al.). The advantage of the use of a regular lattice is obvious: the algorithm for the evolution is much simpler since it does not have to include a complex bookkeeping due to geometry. The first test of our model has been the comparison of the morphological diagrams obtained through simulation to the experimental ones for the bacteria *Proteus mirabilis* and *Bacillus subtilis*. As we have shown it is possible to reproduce the full morphology of the colonies of the two species with a simple adjustment of the parameters of our model. It would be interesting in some future work to confront the results of our model to experimental data in a quantitative way and, perhaps, extract relations between the parameters of the model and the experimental ones.

In this work we took particular care to address, through our simulations, some of the questions that the group of Chuo University has addressed experimentally [58]. The main question, given the variety of the shapes observed in a migrating colony, is

what is controlling this variety. Ideas such as the existence of a pacemaker or some biological mechanism, like chemotaxis, could not obtain experimental confirmation [58, 64]. Thus observations of the lag time of the growth of a colony seed as well as the behaviour of an excised colony annulus led to the conclusion that the main factor responsible for the colony morphology is the local density of bacteria. This is the basic hypothesis that we have built our model upon. The simulations performed, mimicking experimental situations, led to a behaviour of the simulated colony very close to that observed experimentally. Indeed, it has been shown in experiments that the lag phase time depends on the initial cell density, and that there is an upper density threshold where migration phase starts [57, 63, 58, 64], for both *Bacillus subtilis* and *Proteus mirabilis*. Parallely, even if further investigations are needed to clearly confirm it, experiments strongly suggest the existence of a low density threshold that determines the end of the migration phase [58, 64]. There exist already continuous models based on the cell density as a control factor for *Proteus mirabilis* and for *Bacillus subtilis*, with thresholds [36, 39, 40, 46] or without [49, 51]. Our approach is to stick to the automaton approach. Moreover, our model is not only focused on the ring pattern, but is able to reproduce the full variability of the morphological diagram of *Bacillus subtilis*.

In view of the above we may conclude that we are in possession of a quite efficient model for the description of the behaviour of migrating/proliferating bacteria. Several possibilities offer themselves to us at this stage. A first direction to explore would be to try to apply our modelling tools to the description of the morphology of colonies of other bacterial species. The recent experimental progress in this domain is quite substantial and it is now possible to establish detailed morphological diagrams for species not thoroughly studied till recently [59]. Another possibility would be to push towards more quantitative comparisons. To this end we would have first to carefully calibrate our model profiting from the existing reliable experimental data. Once the calibration is successfully completed, we could use the model for quantitative analyses of experiments and, though this may seem a tall order, even predictions. Finally, in a completely different setting, our model could be extended so as to be applicable to the simulation of other processes involving cells. The one that springs to the mind (and one which two of the present authors are familiar with) is the modelling of the growth of solid tumours, where migration plays an important role. Of course, in order to achieve a high degree of realism our model should first be generalised to a three-dimensional one. However this does not

appear unfeasible and in fact we may address the question of tumour modelling in some future work of ours.

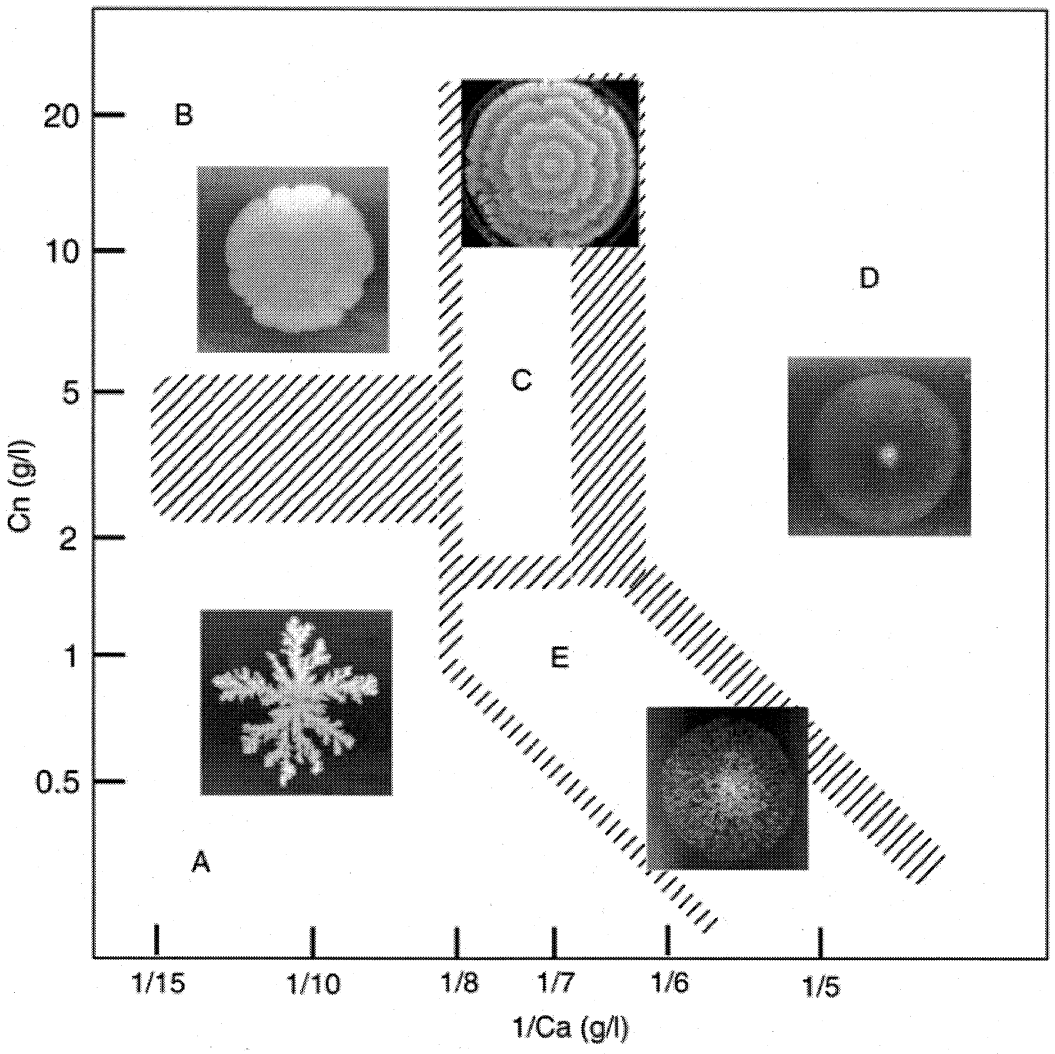

Figure 25: Morphology diagram of *Bacillus subtilis*.

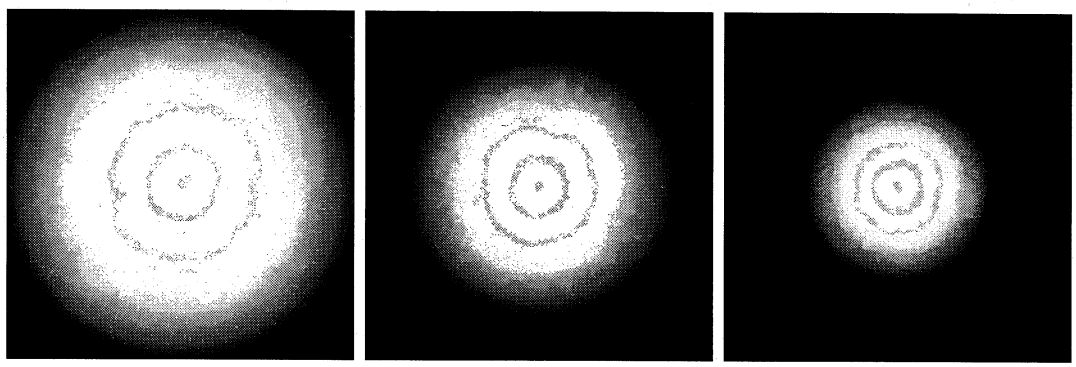

(a) (b) (c)

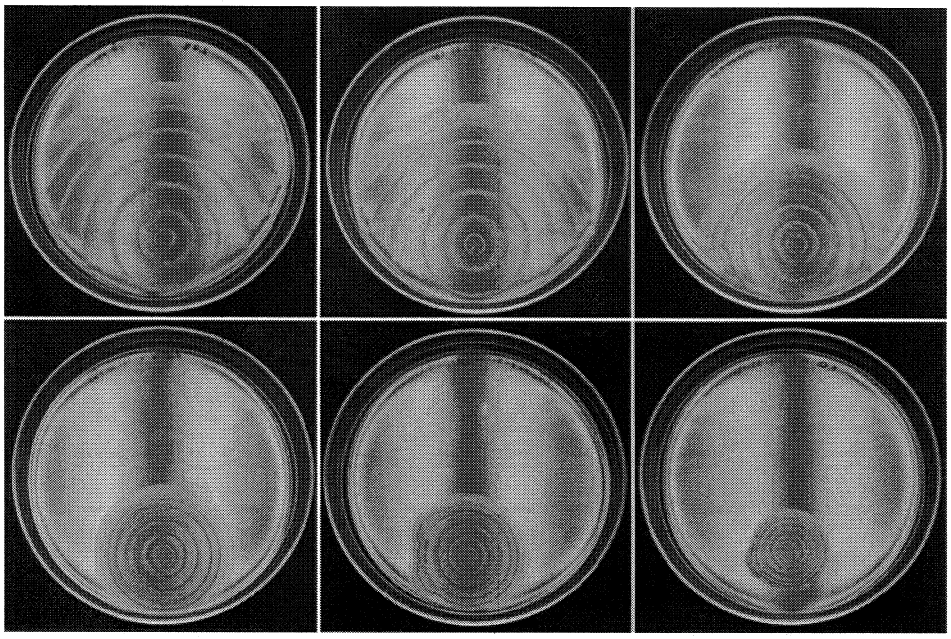

(d)

Figure 26: Ring-like patterns obtained from model B. The parameters are $\alpha = 0.015$, $\beta = 0.0072$, $\Delta_{High} = 300$, $p_{High} = 0.11$, $p_{Low} = 0$, 400×400 cells. (a) $\Delta_{Low} = 10$, 4615 time steps. The growth speed is $v = 4.1 \times 10^{-2}$(cell/step). (b) $\Delta_{Low} = 14$, 3502 time steps. The growth speed is $v = 3.7 \times 10^{-2}$(cell/step). (c) $\Delta_{Low} = 20$, 2631 time steps. The growth speed is $v = 3.3 \times 10^{-2}$(cell/step). (d) Experimental results of effect of agar concentration on colony expansion. The agar concentrations are 2.0, 2.2, and 2.4% (top, left to right) and 2.6, 2.8, and 3.0% (bottom, left to right) [57].

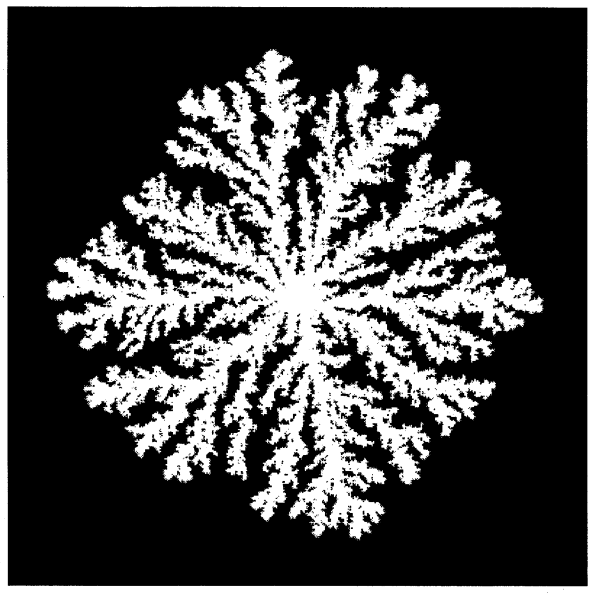

Figure 27: Branch-like structure pattern obtained from model A. The parameters are $\alpha = 0.1$, $\beta = 0.05$, $\gamma = 0.015$, $\lambda = 0.05$, $\Delta_{High} = 100$, $\Delta_{Low} = 22$, $\Delta_n = 5$, $n^0_{i,j} = 20$, $p_b = 0.01$, $p_n = 0.25$, 400×400 cells, 6700 time steps. The growth speed is $v = 2.1 \times 10^{-2}$(cell/step).

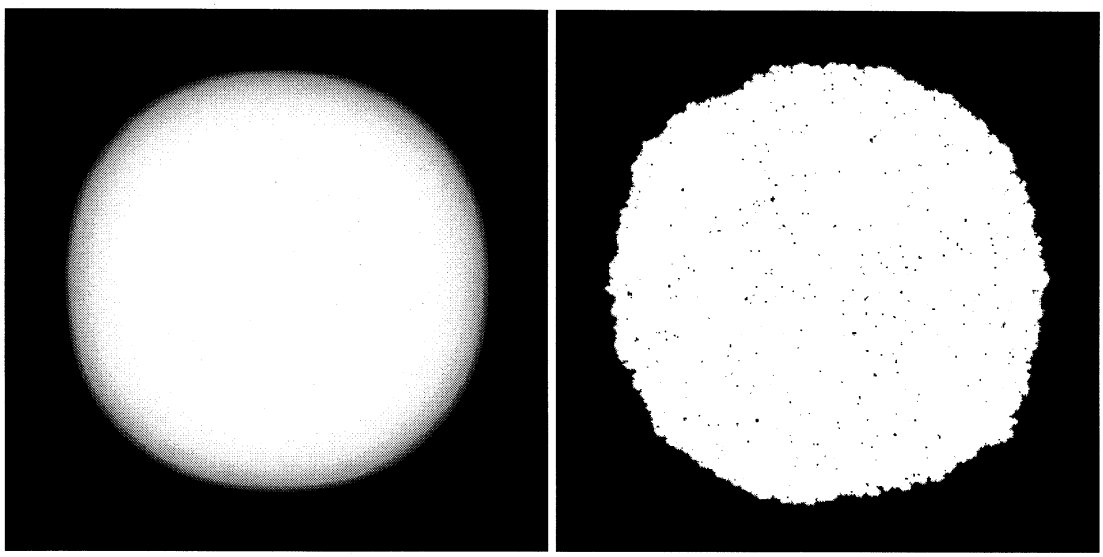

(a) (b)

Figure 28: Eden-like patterns. (a) Model B with the parameters: $\alpha = 0.03$, $\beta = 0.007$, $\Delta_{High} = 200$, $\Delta_{Low} = 65$, $p_{High} = 0.1$, $p_{Low} = 0$, 400×400 cells, 2450 time steps. The growth speed is $v = 5.8 \times 10^{-2}$(cell/step). (b) Model A: $\alpha = 0.6$, $\beta = 0.45$, $\gamma = 0.02$, $\lambda = 0.8$, $\Delta_{High} = 100$, $\Delta_{Low} = 20$, $\Delta_n = 3$, $n^0_{i,j} = 20$, $p_b = 0.05$, $p_n = 0.1$, 400×400 cells, 1750 time steps. The growth speed is $v = 8.9 \times 10^{-2}$(cell/step).

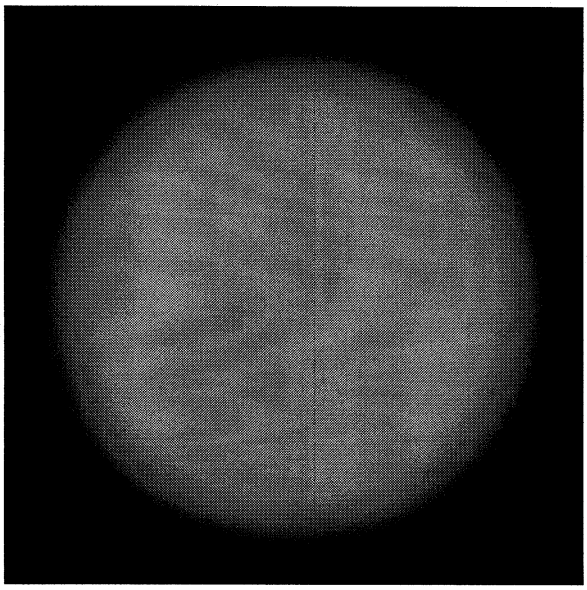

Figure 29: The pattern corresponding to zone D. It is obtained from model A with the parameters: $\alpha = 0.03$, $\beta = 0.025$, $\gamma = 0.01$, $\lambda = 0.1$, $\Delta_{High} = 100$, $\Delta_{Low} = 0$, $\Delta_n = 3$, $n^0_{i,j} = 20$, $p_b = 0.25$, $p_n = 0.1$, 400×400 cells, 1100 time steps. The growth speed is $v = 14.0 \times 10^{-2}$(cell/step). A similar pattern was obtained with model B.

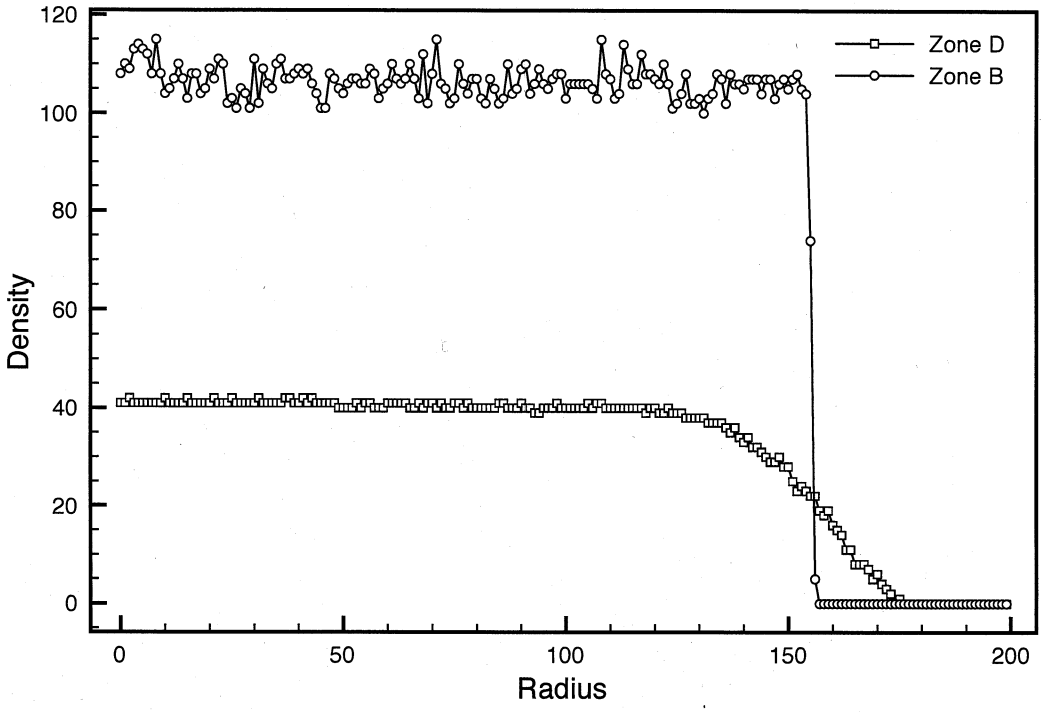

Figure 30: Density profiles corresponding to the patterns of Figure 28b and Figure 29.

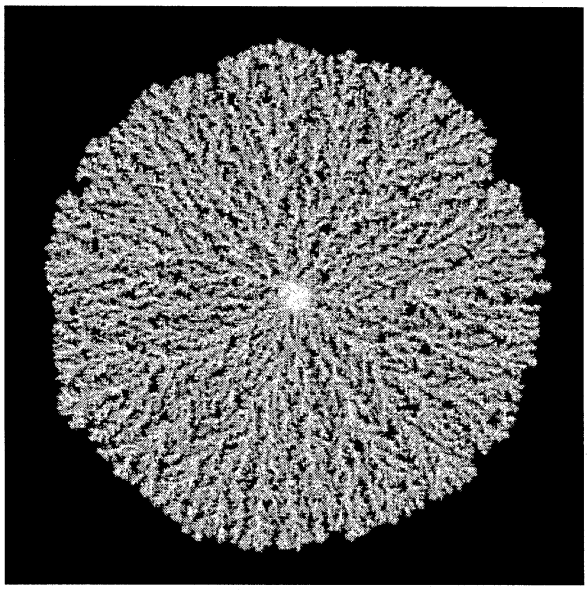

Figure 31: The pattern corresponding to zone E. It is obtained from model A with the parameters: $\alpha = 0.6$, $\beta = 0.45$, $\gamma = 0.15$, $\lambda = 0.8$, $\Delta_{High} = 100$, $\Delta_{Low} = 10$, $\Delta_n = 3$, $n^0_{i,j} = 20$, $p_b = 0.05$, $p_n = 0.1$, 400×400 cells, 1600 time steps. The growth speed is $v = 9.7 \times 10^{-2}$(cell/step).

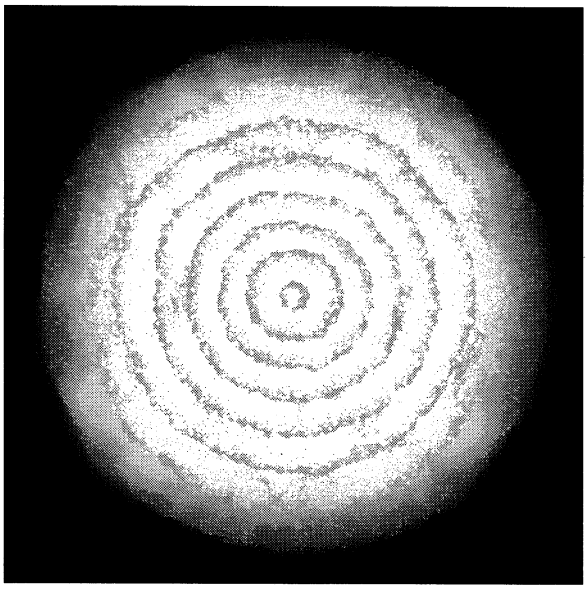

Figure 32: Ring-like pattern obtained from model B with the parameters: $\alpha = 0.015$, $\beta = 0.007$, $\Delta_{High} = 200$, $\Delta_{Low} = 16$, , $p_{High} = 0.1$, $p_{Low} = 0$, 400×400 cells, 4927 time steps. The growth speed is $v = 3.3 \times 10^{-2}$(cell/step).

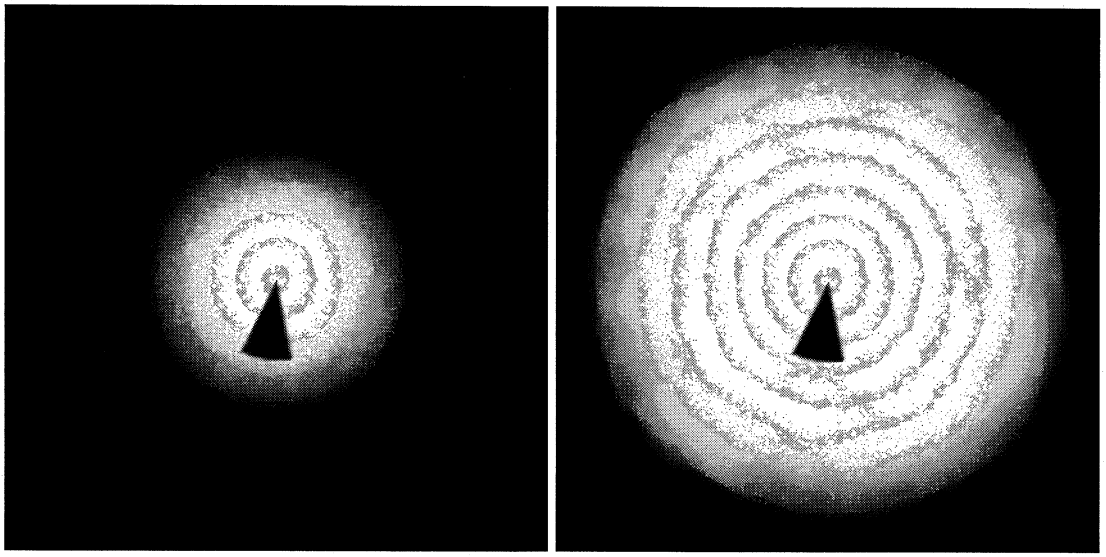

(a) (b)

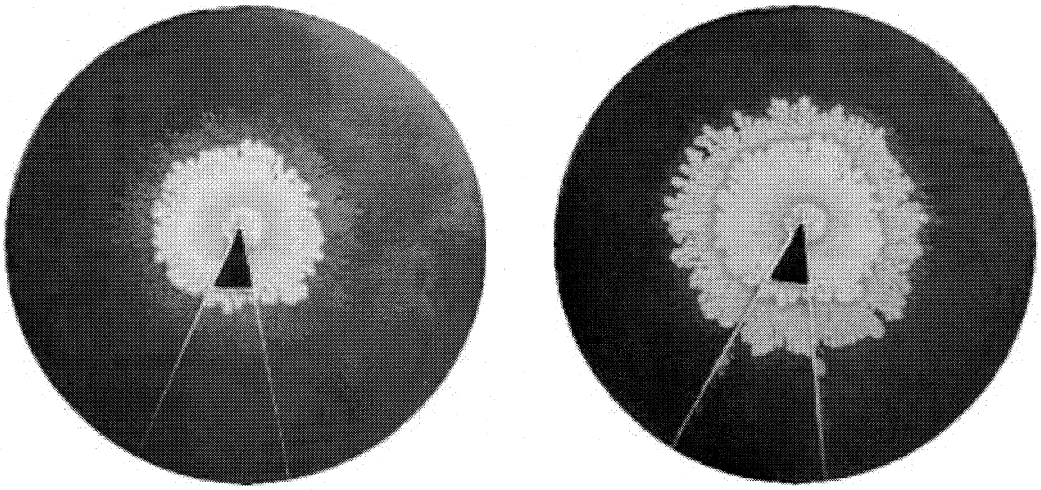

(c) (d)

Figure 33: The time-evolution of the colony (a) 2478 time steps, (b) 5023 time steps after the triangular sector was removed. The pattern was obtained from model B with the parameters: $\alpha = 0.015$, $\beta = 0.007$, $\Delta_{High} = 200$, $\Delta_{Low} = 16$, $p_{High} = 0.1$, $p_{Low} = 0$, 400×400 cells. The growth speed is $v = 3.3 \times 10^{-2}$(cell/step). (c)-(d) Experimental results for the ring-like pattern that removed the triangular sector [58].

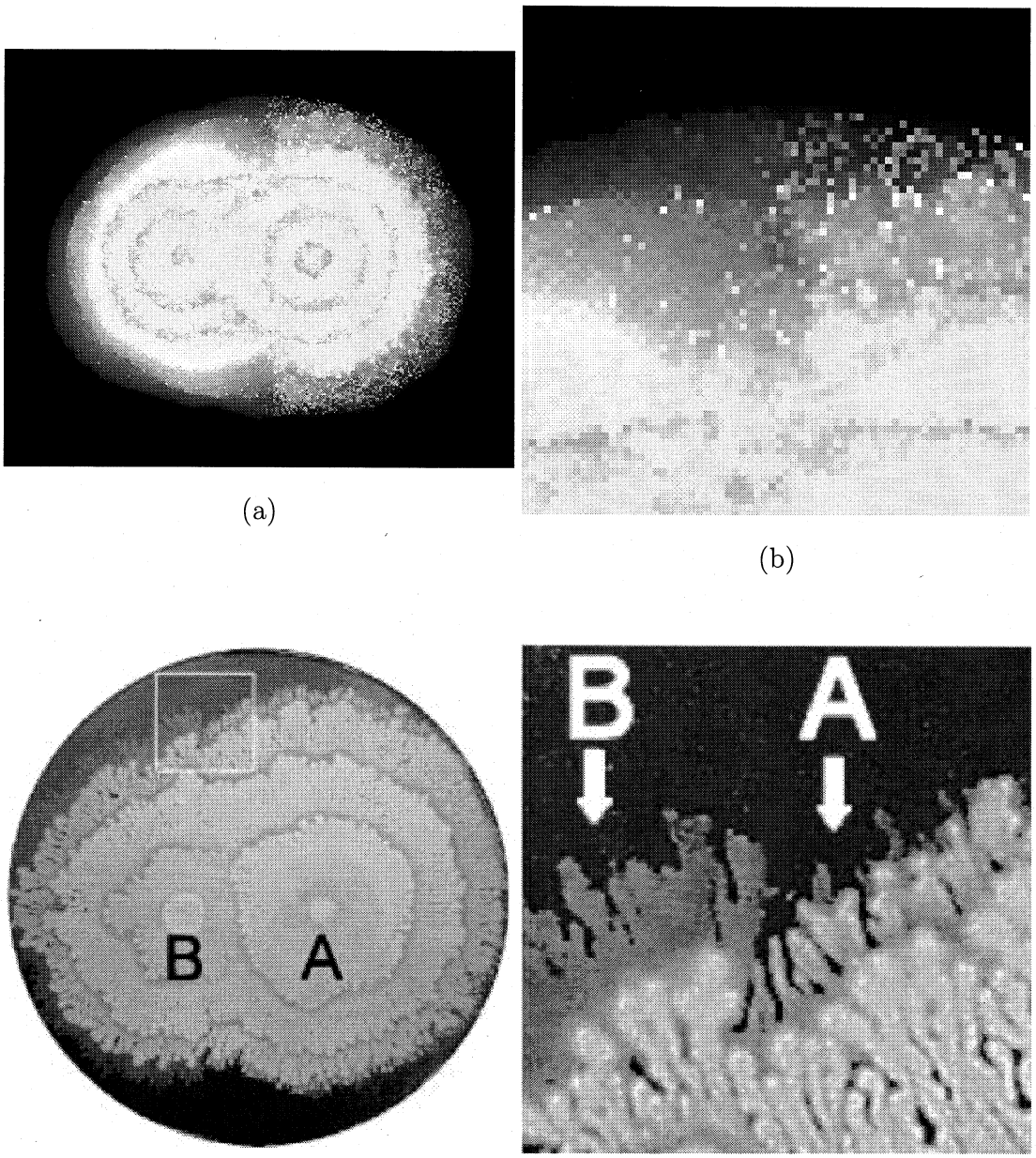

(a) (b)

(c) (d)

Figure 34: Pattern obtained by the collision between two colonies with different phases. The pattern was obtained from model B with the parameters: $\alpha = 0.015$, $\beta = 0.007$, $\Delta_{High} = 200$, $\Delta_{Low} = 17$, $p_{High} = 0.11$, $p_{Low} = 0$. The growth speed is $v = 3.3 \times 10^{-2}$(cell/step). The size of Figure 34a is 270×220 cells, that of (b), the closeup of the boundary of collision, is 70×70 cells. (c)-(d) Experimental results for the possibility of phase entrainment between two colonies with different phase of periodic colony expansion [58].

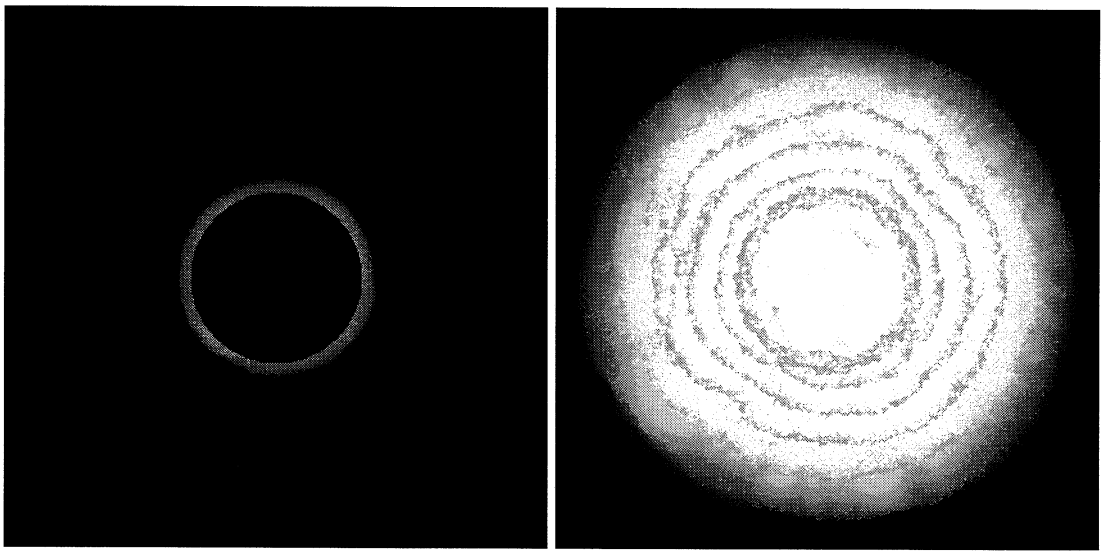

(a) (b)

Figure 35: (a) The initial colony obtained by cutting a ring-like pattern at 1827 time steps. (b) The result at 5493 time steps. They are obtained from model B with the parameters: $\alpha = 0.015$, $\beta = 0.007$, $\Delta_{High} = 200$, $\Delta_{Low} = 16$, $p_{High} = 0.1$, $p_{Low} = 0$, 400×400 cells. The growth speed is $v = 3.3 \times 10^{-2}$(cell/step).

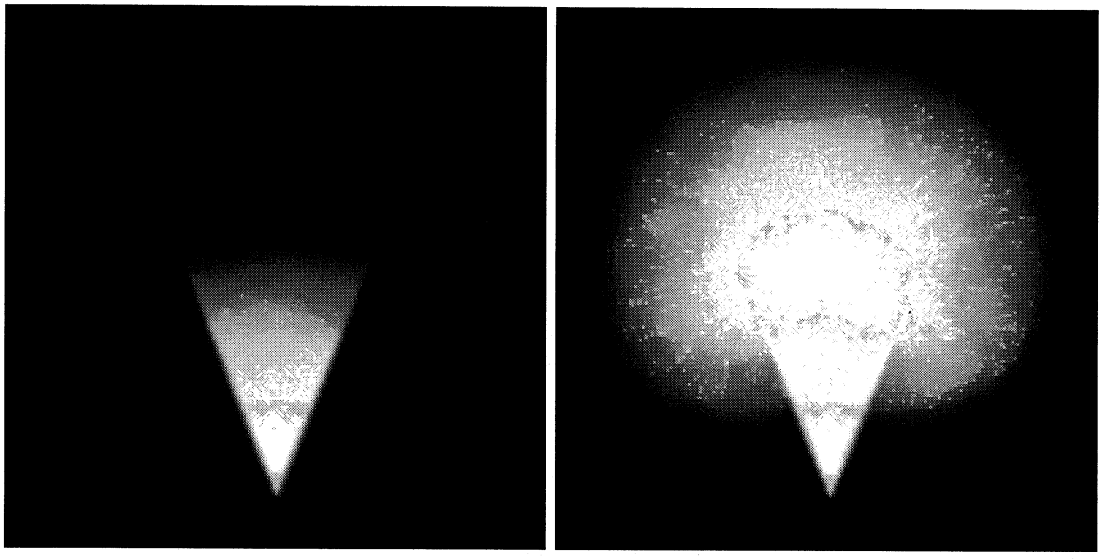

(a) (b)

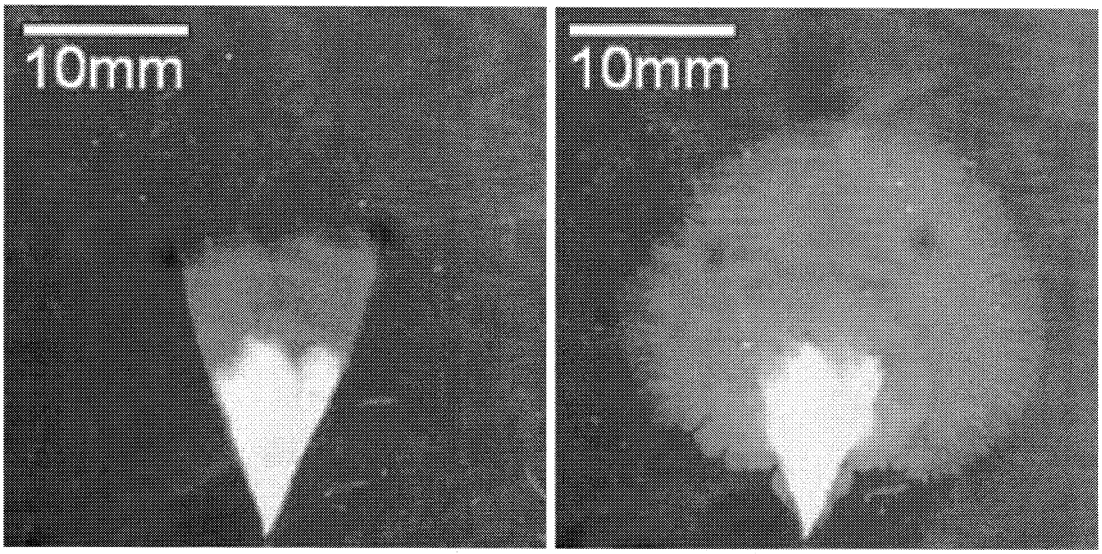

(c) (d)

Figure 36: The initial colony obtained by cutting a triangle-like pattern at 2022 time steps. (b) The result at 4092 time steps. They are obtained from model B with the parameters: $\alpha = 0.015$, $\beta = 0.007$, $\Delta_{High} = 200$, $\Delta_{Low} = 12$, $p_{High} = 0.1$, $p_{Low} = 0$, 200×200 cells. The growth speed is $v = 3.7 \times 10^{-2}(cell/step)$. (c)-(d) Experimental results [58].

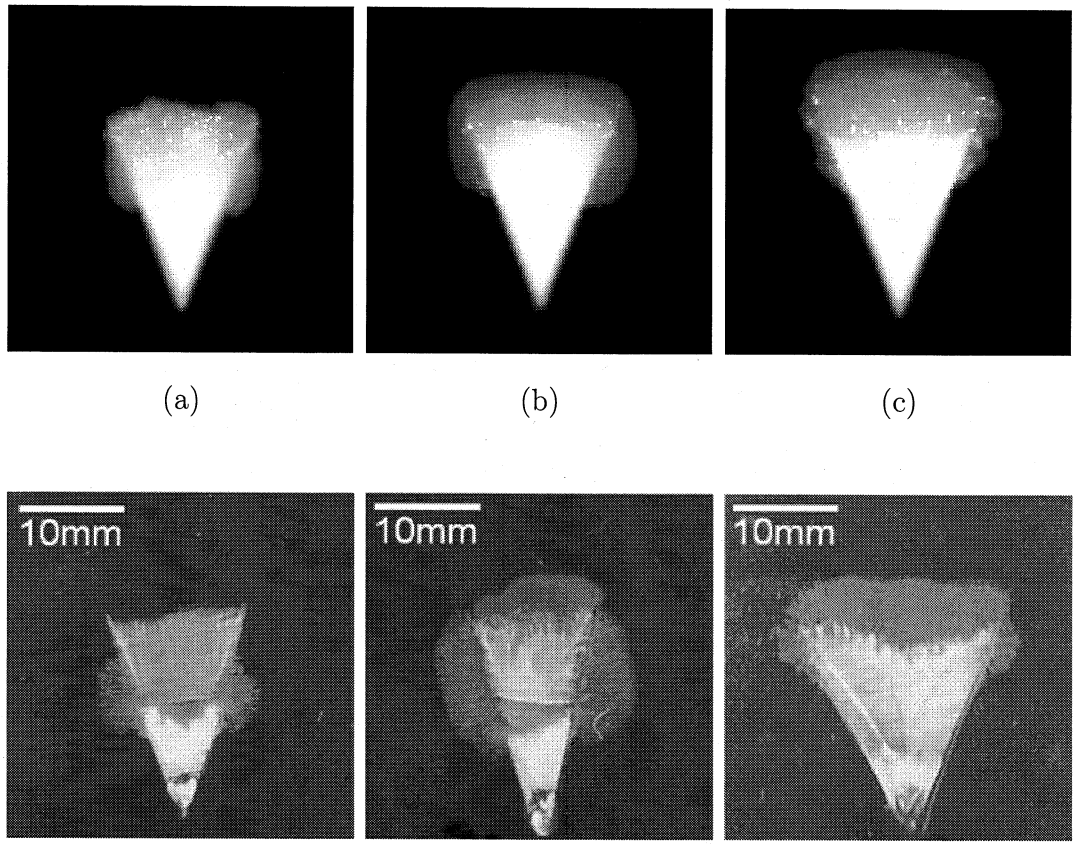

(a) (b) (c)

(d) (e) (f)

Figure 37: (a) Early consolidation phase at 1623 time steps. The colony was cut just after the beginning of the consolidation phase. (b) Middle consolidation phase at 1820 time steps. The colony was cut 183 time steps after the beginning of the consolidation phase. (c) Late consolidation phase at 2101 time steps. The colony was cut 361 time steps after the beginning of the consolidation phase. The patterns were obtained from model B with the parameters: $\alpha = 0.015$, $\beta = 0.007$, $\Delta_{High} = 200$, $\Delta_{Low} = 12$, $p_{High} = 0.1$, $p_{Low} = 0$, 120×120 cells. The growth speed is $v = 3.7 \times 10^{-2}$(cell/step). (d)-(f) Experimental results [58].

Ackowledgments

I would like to express my sincere gratitude to Professor Tetsuji Tokihiro for his continued guidance for doctor thesis completion. When there is no progress in my research I have received his invaluable advice and warm encouragement, and think that it led to my thesis completion. I want to thank to Professor Tetsuji Tokihiro repeatedly. I am deeply grateful to Associate Professor Ralph Willox for a lot of his advices and guidance. He always gives me invaluable guidance when I make some articles in English especially. I also want to thank to Associate Professor Ralph Willox. I am deeply grateful to Associate Professor Hiroshi Tanaka for his continued guidance and encouragement from undergraduate years. "The problem of isotropy" as the main subject of my research was inspired from the discussion with him. I want to thank to Associate Professor Hiroshi Tanaka repeatedly. Professor Basil Grammaticos gives me insightful comments and suggestions. The application to bacterial colonies as chapter 3 of my thesis that was inspired from the discussion with him becomes important part of my thesis. I would like to thank to Professor Basil Grammaticos. Finally, I think that this work was completed by a lot of various supports, encouragements and advices. I would like to take this opportunity to thank to them.

References

[1] J. D. Murray, Mathematical Biology II: Spatial Models and Biomedical Applications, 3rd ed., Springer, New York, 2008.

[2] S. Wolfram, A New Kind of Science, Champaign, Illinois, 2002.

[3] M. Gardner, Wheels, Life and Other Mathematical Amusements, Freeman, New York, 1983.

[4] A. Deutsch and S. Dormann, Cellular Automaton Modeling of Biological Pattern Formation, Birkhäuser, Boston, 2004.

[5] A. N. Zaikin and A. M. Zhabotinsky, Concentration Wave Propagation in Two-dimensional Liquid-phase Self-oscillating System, *Nature* 225 (1970) 535.

[6] R. J. Field and R.M. Noyes, Oscillations in Chemical Systems IV. Limit cycle behavior in a model of a real chemical reaction, *J. Chem. Phys.* 60 (1974) 1877.

[7] J. J. Tyson and P. C. Fife, Target patterns in a realistic model of the Belousov-Zhabotinskii reaction, *J. Chem. Phys.* 73 (1980) 2224.

[8] W. Jahnke and A. T. Winfree, A survey of spiral wave behaviors in the Oregonator model, *Int. J. Bifur. Chaos* 1 (1991) 445.

[9] G. K. Moe, W. C. Rheinboldt and J. A. Abildskov, A computer model of atrial fibrillation, *Am. Heart J.* 67 (1964) 200.

[10] J. M. Greenberg, B. D. Hassard and S. P. Hastings, Pattern formation and periodic structures in systems modeled by reaction-diffusion equations, *Bull. Am. Math. Sot.* 84 (1978) 1296.

[11] J. M. Greenberg and S. P. Hastings, Spatial patterns for discrete models of diffusion in excitable media, *SIAM J. Appl. Math.* 34 (1987) 515.

[12] A. T. Winfree, When Time Breaks Down, Prinston, New Jersey, 1987.

[13] M. Gerhardt, H. Schuster and J. J. Tyson, A cellular automaton model of excitable media: III. Fitting the Belousov-Zhabotinskii reaction, *Physica D* 46 (1990) 416.

[14] M. Markus, Modelling morphogenetic processes in excitable media using cellular automata, *Biomed. Biochim. Acta* 46 (1990) 681.

[15] M. Gerhardt, H. Schuster and J. J. Tyson, A cellular automaton model of excitable media including curvature and dispersion, *Science* 247 (1990) 1563.

[16] M. Gerhardt, H. Schuster and J. J. Tyson, A cellular automaton model of excitable media: II. Curvature, dispersion, rotating waves and meandering waves, *Physica D* 46 (1990) 392.

[17] M. Markus and B. Hess, Isotropic cellular automaton for modelling excitable media, *Nature* 347 (1990) 56.

[18] J. R. Weimar, J.J. Tyson, L.T. Watson, Diffusion and wave propagation in cellular automaton models of excitable media, *Physica D* 55 (1992) 309.

[19] J. R. Weimar, J. J. Tyson and L. T. Watson, Third generation cellular automaton for modeling excitable media, *Physica D* 55 (1992) 328.

[20] C. Henze, J. Tyson, Cellular automaton model of three-dimensional excitable media, *J. Chem. Soc. Faraday Trans.* 92 (1996) 2883.

[21] A. Nishiyama, H. Tanaka and T. Tokihiro, An isotropic cellular automaton for excitable media, *Physica A* 387 (2008) 3129.

[22] J. R. Weimar, Cellular Automata for Reaction Diffusion Systems, *Parallel Computing* 23 (1997) 1699.

[23] R. Kapral, A. Lawniczak, and P. Masiar, Oscillations and waves in a reactive lattice-gas automaton, *Phys. Rev. Lett.* 66 (1991) 2539

[24] S. Chen, S. P. Dawson, G. D. Doolen, D. R. Janecky, and A. Lawniczak, Lattice methods and their applications to reacting systems, *Comput. Chem. Eng.* 19 (1995) 617.

[25] Voronoi G, Nouvelles applications des paramètres continus à la théorie des formes quadratiques, *J. Reine Angew. Math.* 134 (1908) 198.

[26] Badoual M, Derbez P, Aubert M, Grammaticos B, Simulating the migration and growth patterns of *Bacillus subtilis*, *Physica A* 388 (2009) 549.

[27] A. M. Zhabotinsky, Belousov-Zhabotinsky reaction, *Scholarpedia* 2(9) (2007) 1435.

[28] E. Meron, Pattern Formation in Excitable Media, *Phys Rep.* 218 (1992) 1.

[29] N. Dohba, Master Thesis, University of Tokyo, 2000.

[30] H. E. Schepers and M. Markus, Two types of performance of an isotropic cellular automaton: stationary (Turing) patterns and spiral waves, *Physica A* 188 (1992) 337.

[31] T. A. Witten and L. M. Sander, Diffusion-Limited Aggregation, a Kinetic Critical Phenomenon, *Phys. Rev. Lett.* 47 (1981) 1400.

[32] W. Kunishima, A. Nishiyama, H. Tanaka and T. Tokihiro, Differential equations can create complex cellular automaton patterns, *J. Phys. Soc. Jpn.* 73 (2004) 2033.

[33] J. Nagumo, S. Arimoto and S. Yoshizawa, An Active Pulse Transmission Line Simulating Nerve Axon, *Proc. I. R. E.* 50 (1962) 2061.

[34] M. Aubert, M. Badoual, S. Féréol, C. Christo and B. Grammaticos, A cellular automaton model for the migration of glioma cells, *Phys. Biol.* 3 (2006) 93.

[35] M. Aubert, M. Badoual, C. Christov and B. Grammaticos, A model for glioma cell migration on collagen and astrocytes, *J. R. Soc. Interface* 5 (2008) 75.

[36] B. P. Ayati, A structured-population model of *Proteus mirabilis* swarm-colony development, *J. Math. Biol.* 52 (2006) 93.

[37] E. Ben-Jacob, I. Cohen, H. Levine, Cooperative self-organization of microorganisms, *Advances in Physics* 49 (2000) 395.

[38] E. Ben-Jacob, O. Schochet, A. Tenenbaum, I. Cohen, A. Czirók, T. Vicsek, Generic modelling of cooperative growth patterns in bacterial colonies, *Nature* 368 (1994) 46.

[39] A. Czirók, M. Matsushita, T. Vicsek, Theory of periodic swarming of bacteria: application to *Proteus mirabilis*, *Phys. Rev. E* 63 (2001) 031915.

[40] S. E. Esipov, J. A. Shapiro, Kinetic model of *Proteus mirabilis* swarm colony development, *J. Math. Biol.* 36 (1998) 249.

[41] H. Fujikawa, Periodic growth of *Bacillus subtilis* colonies on agar plates, *Physica A* 189 (1992) 15.

[42] B. Grammaticos, M. Badoual, M. Aubert, An (almost) solvable model for bacterial pattern formation, *Physica D* 234 (2007) 90.

[43] H. Itoh, J. Wakita, T. Matsuyama, M. Matsushita, Periodic pattern formation of bacterial colonies, *J. Phys. Soc. Jpn.* 68 (1999) 1436.

[44] K. Kawasaki, A. Mochizuki, M. Matsushita, T. Umeda, Modeling spatio-temporal patterns generated by *Bacillus subtilis*, *J. Theor. Biol.* 188 (1997) 177.

[45] Y. Kozlovsky, I. Cohen, I. Golding, E. Ben-Jacob, Lubricating bacteria model for branching growth of bacterial colonies, *Phys. Rev. E* 59 (1999) 7025.

[46] A. M. Lacasta, I. R. Cantalapiedra, C. E. Auguet, A. Penaranda, L. Ramirez-Piscina, Modeling of spatiotemporal patterns in bacterial colonies, *Phys. Rev. E* 59 (1999) 7036.

[47] J. Lega, T. Passot, Hydrodynamics of bacterial colonies: a model, *Phys. Rev. E* 67 (2003) 031906.

[48] H. Levine, E. Ben-Jacob, Physical schemata underlying biological pattern formation-examples, issues and strategies, *Phys Biol.* 1 (2004) 14.

[49] M. Matsushita, J. Wakita, H. Itoh, I. Rafols, T. Matsuyama, H. Sakaguchi, M. Mimura, Interface growth and pattern formation in bacterial colonies, *Physica A* 249 (1998) 517.

[50] T. Matsuyama, Y. Takagi, Y. Nakagawa, H. Itoh, J. Wakita, M. Matsushita, Dynamic aspects of the structured cell population in swarming colony of *Proteus mirabilis*, *J. Bacteriol.*, 182 (2000) 385.

[51] M. Mimura, H. Sakaguchi, M. Matsushita, Reaction-diffusion modelling of bacterial colony patterns, *Physica A* 282 (2000) 283.

[52] J. Muller, W. Van Saarloos, 2002, Morphological instability and dynamics of fronts in bacterial growth models with nonlinear diffusion, *Phys. Rev. E* 65 (2002) 061111.

[53] A. Nakahara, Y. Shimada, J-I Wakita, M. Matsushita, T. Matsuyama, Morphological diversity of the colony produced by bacteria *Proteus mirabilis*, *J. Phys. Soc. Jpn.* 65 (1996) 2700.

[54] A. Nishiyama and T. Tokihiro, Construction of an isotropic cellular automaton for a reaction-diffusion equation by means of a random walk, submitted to *Physica A*.

[55] I. Rafols (1998) Formation of concentric rings in bacterial colonies, MSc Thesis, Chuo University, Tokyo, Japan. Available at www.sussex.ac.uk/spru/irafols.

[56] M. Ohgiwara, M. Matsushita, T. Matsuyama, Morphological changes in growth phenomena of bacterial colony patterns, *J. Phys. Soc. Jpn.* 61 (1992) 816.

[57] O. Rauprich, M. Matsushita, C. J. Weijer, F. Siegert, S. E. Esipov, J. A. Shapiro, Periodic phenomena in *Proteus mirabilis* swarm colony development *J. Bacteriol.*, 178 (1996) 6525.

[58] H. Shimada, T. Ikeda, J. Wakita, H. Itoh, S. Kurosu, F. Hiramatsu, M. Nakatsuchi, Y. Yamazaki, T. Matsuyama, M. Matsushita, Dependence of local cell density on concentric ring colony formation by bacterial species *Bacillus subtilis*, *J. Phys. Soc. Jpn.* 73 (2004) 1082.

[59] R. Tokita, T. Katoh, Y. Maeda, J. Wakita, M. Sano, T. Matsuyama, M. Matsushita, Pattern formation of bacterial colonies by *Escherichia coli*, *J. Phys. Soc. Jpn.* 78 (2009) 074005.

[60] T. Vicsek, M. Cserzo, V. K. Horvath, Self-affine growth of bacterial colonies, *Physica A* 167 (1990) 315.

[61] J. Wakita, K. Komatsu, A. Nakahara, T. Matsuyama, M. Matsushita, Experimental investigation on the validity of population dynamics approach to bacterial colony formation, *J. Phys. Soc. Jpn.* 63 (1994) 1205.

[62] J. Wakita, I. Rafols, H. Itoh, T. Matsuyama, M. Matsushita, Experimental investigation on the formation of dense-branching-morphology-like colonies in bacteria, *J. Phys. Soc. Jpn.* 67 (1998) 3630.

[63] J. Wakita, H. Shimada, H. Itoh, T. Matsuyama, M. Matsushita, Periodic colony formation by bacterial species *Bacillus subtilis*, *J. Phys. Soc. Jpn.* 70 (2001) 911.

[64] Y. Yamazaki, T. Ikeda, H. Shimada, F. Hiramatsu, N. Kobayashi, J. Wakita, H. Itoh, S. Kurosu, M. Nakatsuchi, T. Matsuyama, M. Matsushita, Periodic growth of bacterial colonies, *Physica D* 205 (2005) 136.